The Influence of a Superconducting Split-pair Solenoid as an Insertion Device on the Performance of a Storage Ring for Synchrotron Radiation

T. Hezel, B. Krevet, H. O. Moser,
R. Rossmanith

Projekt Mikrosystemtechnik

Forschungszentrum Karlsruhe

Technik und Umwelt

Wissenschaftliche Berichte

FZKA 5839

The Influence of a Superconducting Split-pair Solenoid as an Insertion Device on the Performance of a Storage Ring for Synchrotron Radiation

T. Hezel, B. Krevet, H. O. Moser, R. Rossmanith

Projekt Mikrosystemtechnik

THE INFLUENCE OF A SUPERCONDUCTING SPLIT-PAIR SOLENOID AS AN INSERTION DEVICE ON THE PERFORMANCE OF A STORAGE RING FOR SYNCHROTRON RADIATION

Abstract

In order to push the photon energies to higher values strong and highly nonlinear magnets are considered to be installed in synchrotron radiation storage rings. These magnets can seriously affect the operation of the storage ring both by increasing the emittance and by reducing the dynamic aperture. In this paper a technique based on Lie-algebra is described which allows to calculate the influence of nonlinear fields on the dynamic aperture. This technique is applied to study the influence of a 12 T wavelength shifter based on commercially available split-pair solenoid magnets on the future synchrotron radiation source ANKA.

EINFLUSS EINES ALS INSERTION DEVICE VERWENDETEN SUPRALEITENDEN SPLIT-PAIR SOLENOIDEN AUF DAS VERHALTEN EINES SPEICHERRINGES FÜR SYNCHROTRONSTRAHLUNG

Übersicht

Zur Erhöhung der Photonenenergie von Synchrotronstrahlungsquellen wird die Verwendung von starken nichtlinearen Magneten in Betracht gezogen. Solche Magnete können einen starken Einfluß auf die Funktion von Speicherringen ausüben, da sie die Emittanz vergrößern und die dynamische Apertur verringern können. In der vorliegenden Arbeit wird eine Methode vorgestellt, mit deren Hilfe der Einfluß der nichtlinearen Felder auf die dynamische Apertur berechnet werden kann. Mit dieser Methode wird die mögliche Auswirkung eines als Wellenlängenschieber eingesetzten kommerziellen 12 T Split-pair Solenoiden auf die dynamische Apertur der zukünftigen Synchrotronstrahlungsquelle ANKA untersucht.

Contents

I. Introduction

Electron storage rings for synchrotron radiation are becoming a more and more important tool in basic research, materials research and Applied Physics. The wavelength of the emitted synchrotron radiation is defined by the particle energy and the magnetic field in which the synchrotron radiation is generated: the higher the energy and the magnetic field the higher the energy of the emitted photons. The energy of the beam defines the cost of the accelerator. Hence, there is a tendency to build synchrotron light sources with the lowest possible beam energy and to install high field superconductive magnets (so-called wavelength shifters) in certain positions of the accelerator [1].

The high field insertion devices may strongly influence the behavior of the beam. In most cases the fields are extremely nonlinear and may reduce the stability of the storage ring. It is therefore necessary to simulate the influence of these elements on beam stability.

In a storage ring particle trajectories have to be stable over hours. Whenever the electrons are emitting photons they loose energy and, as a result, have a tendency to leave the main trajectory in the bending magnets. In order to maintain the beam, the particles have to be confined by quadrupoles (focusing magnetic elements) distributed in the ring. The particles are bounced back by these focusing elements when they try to escape.

Quadrupoles not only confine the beam but can also be a source of instability. Whenever a particle tries to escape, the quadrupoles distributed along the ring force it to oscillate around the ideal trajectory. It is convenient to approximate this oscillation by a pseudo-sinusoidal motion. In this approximation the number of wavelengths per revolution is the Q-value (or ν value) of the machine. When the Q-value is an integer or half an integer small magnetic misalignments can increase the amplitude of the oscillations from revolution to revolution: the beam is unstable. In order to avoid this instability, the strength of the quadrupoles has to be chosen in such a way that the beam is far away from resonances.

The quadrupoles have a field which increases linearly with the distance from the main trajectory. Magnetic elements can also have in addition to the linear term, a quadratic or cubic term. The nonlinear elements produce additional resonances and limit the area of stable Q-values even more.

The nonlinear field components generate an additional problem. The strength of the restoring force depends on the distance from the main trajectory in a nonlinear way. Particles with large deviations from the main trajectory have a different Q-value than particles with a small betatron amplitude. In other words, particles with large amplitudes can become unstable.

The border between the region where the particles are still stable and the region where the particles do not find a stable trajectory is called dynamic aperture. In general the dynamic aperture is much smaller than the aperture given by the vacuum chamber.

The dynamic aperture can be calculated by tracking particles with different distances and angles relative to the design orbit over many revolutions. If the accelerator consists exclusively of standard magnets (bending magnets, quadrupoles and sextupoles) simple tracking techniques can be used. When the accelerator contains elements with complicated field patterns, as for example the above mentioned wavelength shifter, this simple technique fails.

In order to solve this problem a Lie-algebra based approach is described in this paper [2]. Each magnetic element is described by a so-called map. This map describes the linear and the nonlinear change of the particle trajectory caused by an element when the particle goes through it.

MARYLIE [3] which is used in the approach presented in this paper is a standard program that uses this Lie map technique for standard magnets like bending magnets, quadrupoles etc. For unconventional magnets, like the superconductive wavelength shifter, two programs, ORBIT and LIEMAP [4], were developed which calculate the transfer map for elements with arbitrary magnetic fields. MARYLIE integrates the map into its total transfer map and calculates the dynamic aperture of the whole accelerator [5].

ORBIT calculates and optimizes the design orbit through the unknown field element. The field is calculated by using the magnet program TOSCA [6]. Afterwards LIEMAP calculates the map for the optimized orbit.

In the course of the paper these programs are used to calculate the influence of a wavelength shifter on the dynamic aperture of the synchrotron light source ANKA (2.5 GeV) [7]. The wavelength shifter has a maximum field of 12 Tesla (normal bending magnet 1.5 Tesla). The high field is obtained by superconductive solenoid coils both above and below the trajectory (so-called split pair solenoids). The field of this magnet is highly nonlinear.

II. Lie Algebra and symplectic tracking, a short overview

The following short overview over the Lie algebra formalism relies almost exclusively on the work of Dragt and coworkers [2] which might be consulted for more detail.

a. The equation of motion

The action of an electromagnetic field on a particle is described by Hamilton's equations

$$dq_i/dt = \partial H/\partial p_i$$
$$dp_i/dt = - \partial H/\partial q_i \qquad (i = 1,2,3) \qquad (1)$$

in which $(q_1,q_2,q_3,p_1,p_2,p_3)$ are the generalized coordinates and momenta of the particle. H is the Hamiltonian

$$H(x,y,z,p_x,p_y,p_z;t) = \{m_0^2c^4 + c^2[(p_x\text{-}eA_x)^2 + (p_y\text{-}eA_y)^2 + (p_z\text{-}eA_z)^2] \}^{\frac{1}{2}} + e\phi \qquad (2)$$

where $A = (A_x, A_y, A_z)$ is the vector potential, ϕ the scalar potential, m_0 the rest mass and e the elementary charge.

In particle tracking time is not such an important variable as is z, the coordinate in the direction of motion. Therefore a new Hamiltonian of the form $K(x,y,t,p_x,p_y,p_t;z)$ is chosen, in which z is the new independent variable. Hamilton's equations are now

$$dq_i/dt = \partial K/\partial p_i$$
$$dp_i/dt = - \partial K/\partial q_i \qquad (i = 1,2,3) \qquad (3)$$

and the Hamiltonian K is

$$K(x,y,t,p_x,p_y,p_t;z) = \left(\frac{(p_t + e\phi)^2}{c^2} - m_0^2c^2 - (p_x - eA_x)^2 - (p_y - eA_y)^2 \right)^{\frac{1}{2}} - eA_z \qquad (4)$$

3

In order to describe the action of a magnetic element the generalized coordinates and momenta at the exit have to be correlated with those at the entrance. This can be done by integrating many individual trajectories or by calculating the so-called transfer map M:

$$\vec{z}^{\,fin} = M \, \vec{z}^{\,in} \tag{5}$$

b. Symplectic tracking

When the direction of the transformation (5) is reversed, $\vec{z}^{\,fin}$ has to be transformed into $\vec{z}^{\,in}$. In general a small change in the initial conditions causes a change in the final conditions.

$$M_{ab} (\vec{z}^{\,in}) = \partial z_a^{\,fin} / \partial z_b^{\,in} \tag{6}$$

The elements of the map M_{ab} depend in general on the elements of the vector $\vec{z}^{\,in}$. A matrix J is defined

$$J = \begin{pmatrix} 0 & I \\ -I & 0 \end{pmatrix} \tag{7}$$

where I is a 3 x 3 identity matrix. $\widetilde{M}$ is the transposed matrix of M and the condition for symplecticity is:

$$\widetilde{M}(\vec{z}^{\,in}) \, J \, M(\vec{z}^{\,in}) = J \tag{8}$$

J is independent of $\vec{z}^{\,in}$ despite the fact that the matrix M depends on $\vec{z}^{\,in}$. This is the symplectic condition.

c. Lie transformation and symplecticity

Starting point is the six-dimensional phase space $(q_1,q_2,q_3,p_1,p_2,p_3;t)$. When f is any variable of the phase space coordinates $f(q,p)$, df/dt can be calculated by the chain rule

$$df/dt = \sum_{i=1}^{3} (\partial f/\partial q_i)dq_i/dt + (\partial f/\partial p_i)dp_i/dt = \sum_{i=1}^{3} (\partial f/\partial q_i)(\partial H_i/\partial p_i) - (\partial f/\partial p_i)(\partial H_i/\partial q_i) \qquad (9)$$

The right hand side of the equation is calculated by using equation (1).
The Poisson bracket is defined in the following way

$$[f,g] = \sum_{i=1}^{3} (\partial f/\partial q_i)(\partial g/\partial p_i) - (\partial f/\partial p_i)(\partial g/\partial q_i) \qquad (10)$$

With this definition df/dt is

$$df/dt = [f,H] \qquad (11)$$

In association with any function f a Lie operator :f: is defined which acts on the function g in the following way

$$:f:g = [f,g] \qquad (12)$$

A Lie transformation, symbolically written as $\exp(:f:)$, is defined as

$$\exp(:f:) = \sum_{m=0}^{\infty} \frac{:f:^{m}}{m!} \qquad (13)$$

More explicitly, the action of a Lie transformation on the function z_a is written as

$$\exp(:f:) z_a = z_a + [f,z_a] + [f,[f,z_a]]/2! + \ldots\ldots \qquad (14)$$

5

The theory shows that M

$$M = \exp(:f_2:) \exp(:f_3:) \exp(:f_4:) \ldots\ldots \quad (15)$$

is symplectic when f_n is a polynomial of degree n. This property can be used to track particles through complex fields over many revolutions.

A simple example shows this. As written usually a sextupole changes the particle trajectory in the following way (for $y_0 = 0$, $y_0' = 0$):

$$x = x_0$$
$$x' = ax_0^2 + x_0' \quad (16)$$

The function $f_3 = sq^3/3$ used as Lie operator yields

$$\exp(:f_3:)q = q$$
$$\exp(:f_3:)p = p + sq^2 \quad (17)$$

Equation (16) and (17) are of the same form. The sextupole can be described by the polynomial of the third order. A polynomial of the fourth order describes an octupole etc. With this technique the influence of beam line elements with arbitrary fields can be predicted. Dragt et al. developed differential equations for the polynomials f_2, f_3 and f_4. Integrating them along the design orbit and putting the results in equation (15) yields the whole map describing the action of a beamline element in our case up to order 3 in the coordinates.

The map of a beamline element with arbitrary field is read by the program MARYLIE. It is used to calculate the linear and nonlinear properties of the accelerator structure and the dynamic aperture.

The calculations have to be performed in three steps:

    I.   The design orbit through the nonlinear beamline element has to be calculated. This is done by the program ORBIT.

    II.   Once the design orbit is known the coefficients for the polynomials have to be evaluated and the map calculated. This is done by the program LIEMAP.

III. The map is read into MARYLIE which gives the optical properties and the dynamic aperture.

III. Numerical Calculation of the Trajectory

In order to calculate the trajectory the differential equations (1) have to be solved numerically. This is done in the usual way by defining a mesh. At the mesh points the field and its derivatives are calculated by a standard magnet program like TOSCA [6]. The field strength and the corresponding derivatives are stored in a table.

In order to reduce the number of stored values a trajectory is chosen which is not too far away from the expected trajectory. How this is done is explained in the chapter which describes the program ORBIT. The fields values, the derivatives and the interpolation parameters are stored in this table and used for the integration.

The numerical solution is performed with the help of a Runge-Kutta integration as a start-up procedure followed by an Adams-Moulton predictor-corrector method. Both techniques are well described in the literature [8]. In principle a predictor-corrector method approximates the trajectory by two different formulae. One is used for prediction and the other one for correction.

With the Runge-Kutta method the ordinary differential equation $y' = f(x,y)$ or a set of differential equations is solved for given initial conditions x_0, y_0, z_0. In the literature advanced Runge-Kutta algorithms are described which solve the equation of motions numerically. For our calculations we use a 13th order Runge-Kutta approximation developed by Fehlberg [8]. The exact solutions for one point (x_0, y_0) must be known. The solution in the vincinity of this point is calculated by a Taylor expansion. The solution of the equation for the point (x_{n+1}, y_{n+1}) is derived from the point (x_n, y_n).

$$y_{n+1} = y_n + A_{i\,1} K_1 + ... + A_{i\,8} K_8$$

where the K_i's are

$$K_i = h\, f(x_n + \vartheta_i h,\, y_n + A_{i\,1} K_1 + ... + A_{i\,i\text{-}1} K_{i\text{-}1}) \qquad (18)$$

7

h is the stepsize. The A_{ij}'s and ϑ_i's are coefficients summarized in Appendix II.

The Runge-Kutta-Fehlberg integration is used as a start-up procedure. After calculating the six phase variables for 10 points the Adams-Moulton procedure starts. The Adams-Moulton method is based on the idea of numerical integration:

$$y(x_{n+1}) = y(x_n) + \int_{x_n}^{x_{n+1}} f(x,y)dx \qquad (19)$$

When already approximate solutions for equally spaced points exist a recursive formula minimizes the difference. This calculation requires only one evaluation of the function f(x,y) per step and is therefore very fast.

The recursion formula for the predictor is:

$$y_{n+1} = y_n + \frac{h}{72576 \cdot 10^2} \cdot \Big[30277247 \cdot \hat{y}_n - 104995189 \cdot \hat{y}_{n-1} + 265932680 \cdot \hat{y}_{n-2}$$
$$454661776 \cdot \hat{y}_{n-3} + 538363838 \cdot \hat{y}_{n-4}$$
$$444772162 \cdot \hat{y}_{n-5} + 252618224 \cdot \hat{y}_{n-6}$$
$$94307320 \cdot \hat{y}_{n-7} + 20884811 \cdot \hat{y}_{n-8}$$
$$2082753 \cdot \hat{y}_{n-9} \Big]. \qquad (20)$$

Since this solution is not exact y_{n+1} is fed in the equation of motion and a new value $\hat{y}_{n+1}$ is calculated. The corrector formula is:

$$y_{n+1} = y_n + \frac{h}{72576 \cdot 10^2} \cdot \Big[2082753 \cdot \hat{y}_{n+1} + 9449717 \cdot \hat{y}_n - 11271304 \cdot \hat{y}_{n-1}$$
$$16002320 \cdot \hat{y}_{n-2} - 17283646 \cdot \hat{y}_{n-3}$$
$$13510082 \cdot \hat{y}_{n-4} - 7394032 \cdot \hat{y}_{n-5}$$
$$2687864 \cdot \hat{y}_{n-6} - 583435 \cdot \hat{y}_{n-7}$$
$$57281 \cdot \hat{y}_{n-8} \Big]. \qquad (21)$$

Using the stored results of the Runge-Kutta calculation (points 0 to 9) the Adams-Moulton predictor calculates point number 10 (fig. 1) of the trajectory (20).
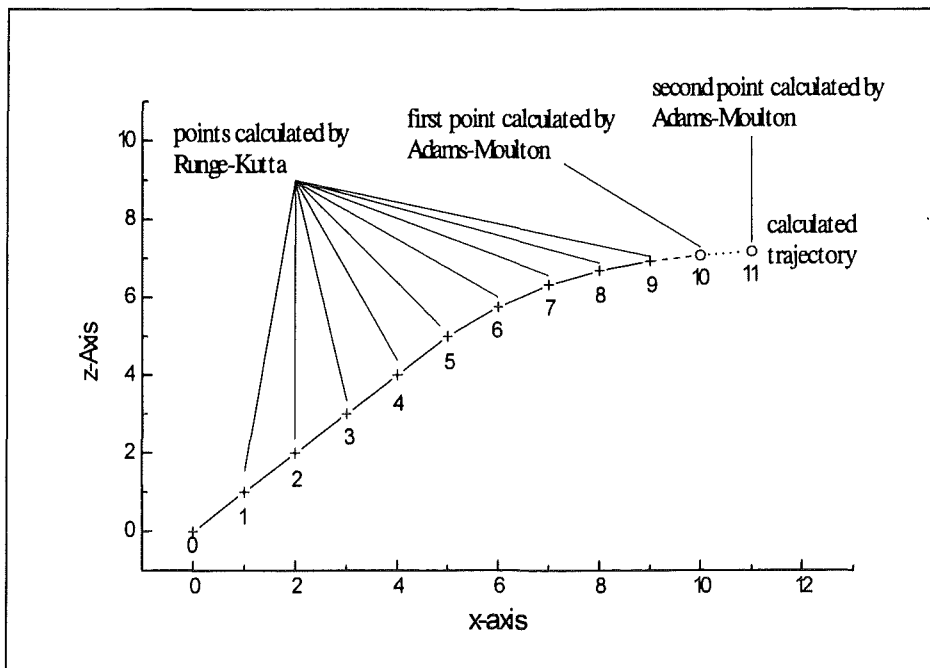
Fig. 1: Runge-Kutta start-up and Adams-Moulton predictor-corrector method.

The Adams-Moulton corrector method recalculates the 10th point. The results for the 10th point are now determined more exactly. This procedure is carried out 4 times and afterwards the results are stored.

In order to calculate the 11th point the procedure starts again. Now points 1 to 10 are used by the Adams-Moulton predictor to calculate the next point.

When the trajectory is found, the field strength and the field derivatives along the trajectory are interpolated. The program has an optimization routine which means that the calculations can be repeated with different starting conditions in order to optimize a certain parameter of the beamline element, for instance the deflecting angle.

In the following, the use of the program is demonstrated by calculating the influence of a wavelength shifter (split pair solenoid) on the dynamic aperture of the storage ring ANKA.

IV. The field of the superconducting split pair solenoid magnet

Our calculations are based on a commercially available superconductive split pair solenoid. In order to obtain a high field (e.g. 12 T) the magnet consists of eight coils. This arrangement is shown in fig. 2 [9]. Fig. 3 shows the magnetic field of each of these coils as calculated with the program TOSCA. In this figure only the right hand side of the magnetic field is shown (starting from the center).
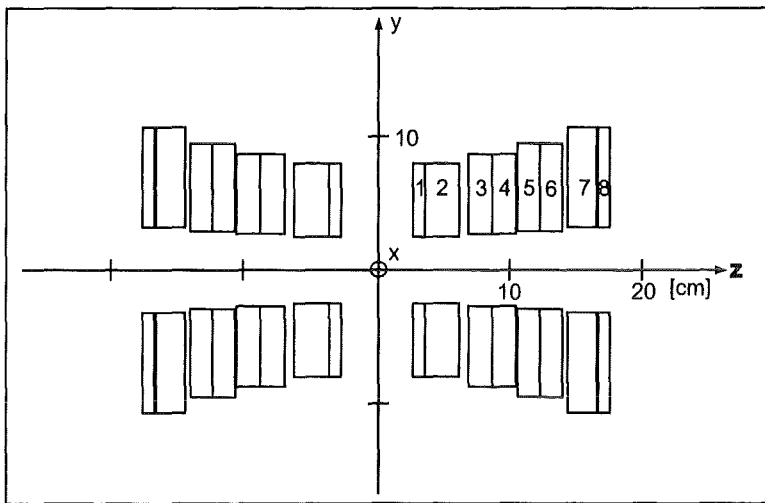
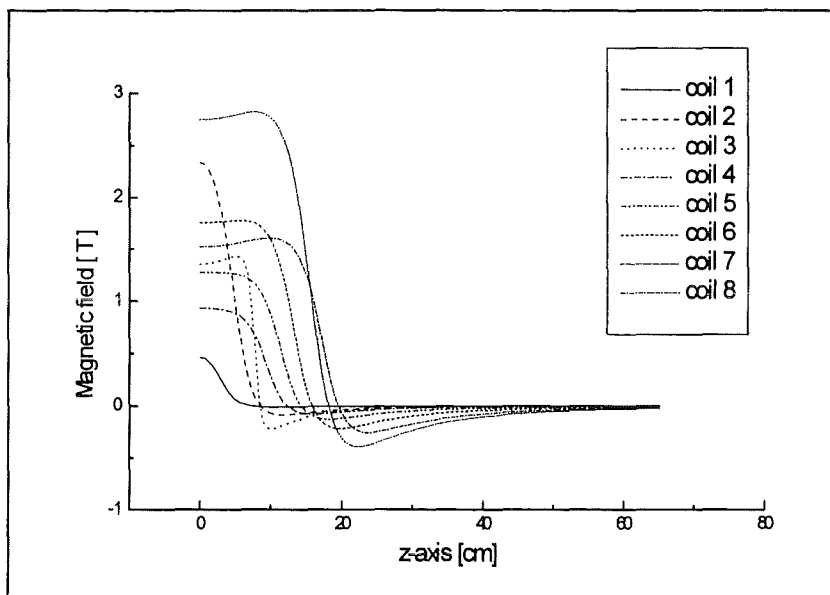Fig. 2: The arrangement of the eight coils. z is the direction of the beam.

Fig. 3: The field contribution of the individual coils.

The result of the superposition of the individual fields is shown in fig. 4. The field has a dip in the vicinity of 8 T which is a property of this specific coil arrangement. For other coil arrangements the field could be different. The negative field is almost 1T.

In order to arrive at a better understanding of the field's action on the particle trajectory, it is convenient to expand the field in quadrupole, sextupole and octupole components in the plane perpendicular to the z-axis:

$$B(r,z,\theta) = \sum_{n=1}^{5} \frac{a_n(z) \cdot r^{n-1} \cdot \cos n\theta}{n!} \qquad (22)$$

a_n is the so-called "Fourier coefficient" at each point, r is the distance from the z-axis. θ is 0 in the following calculations.
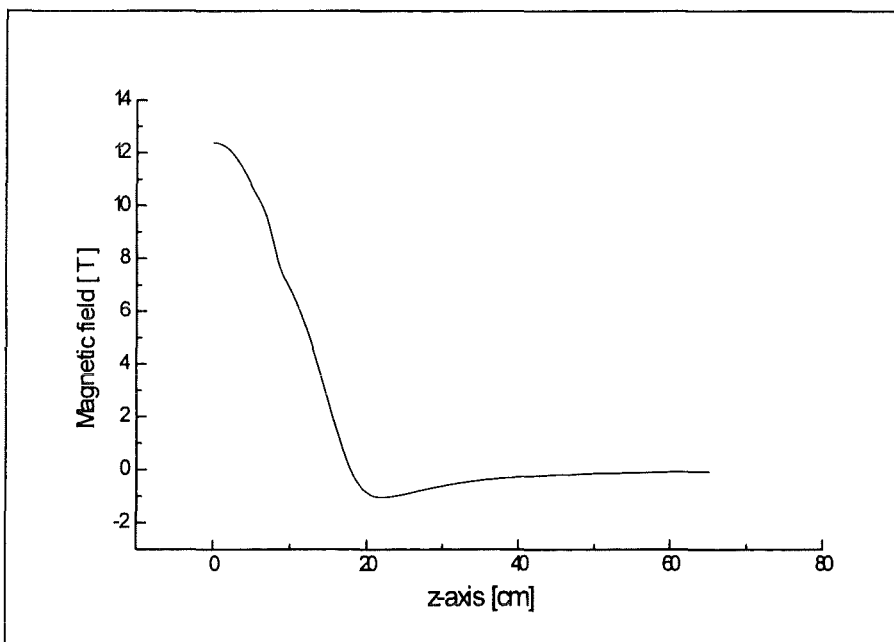

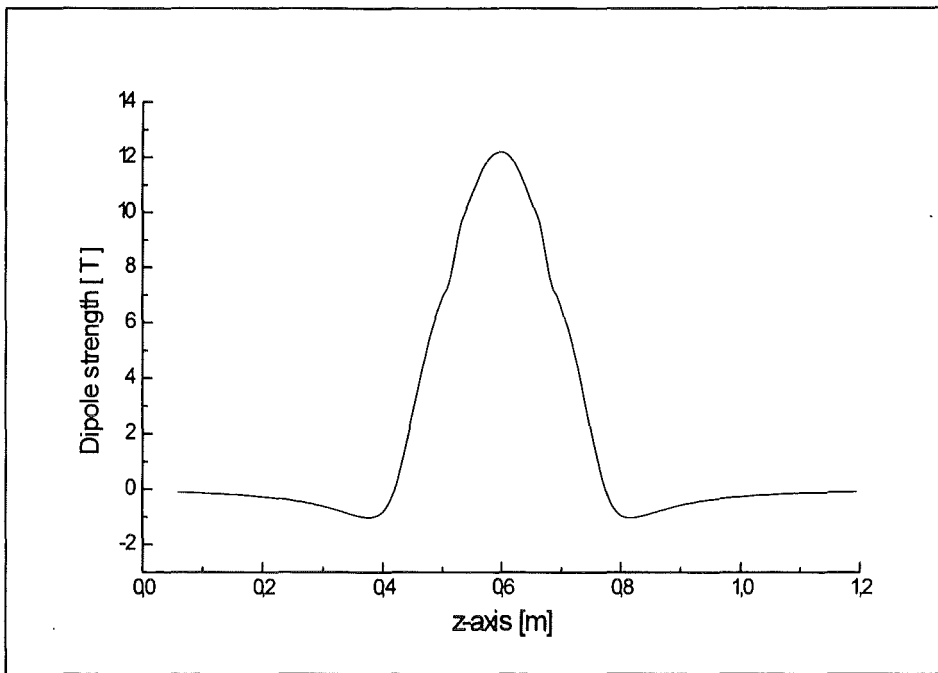Fig. 4: Superposition of the fields from the individual coils from fig. 3.

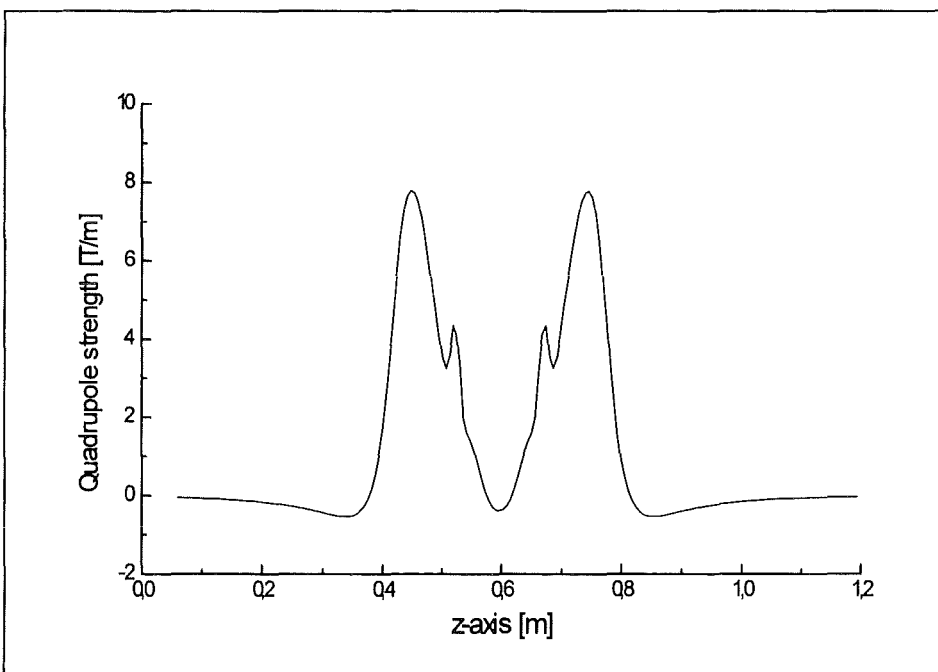Fig. 5: Dipole coefficient a_1 as defined in (22).

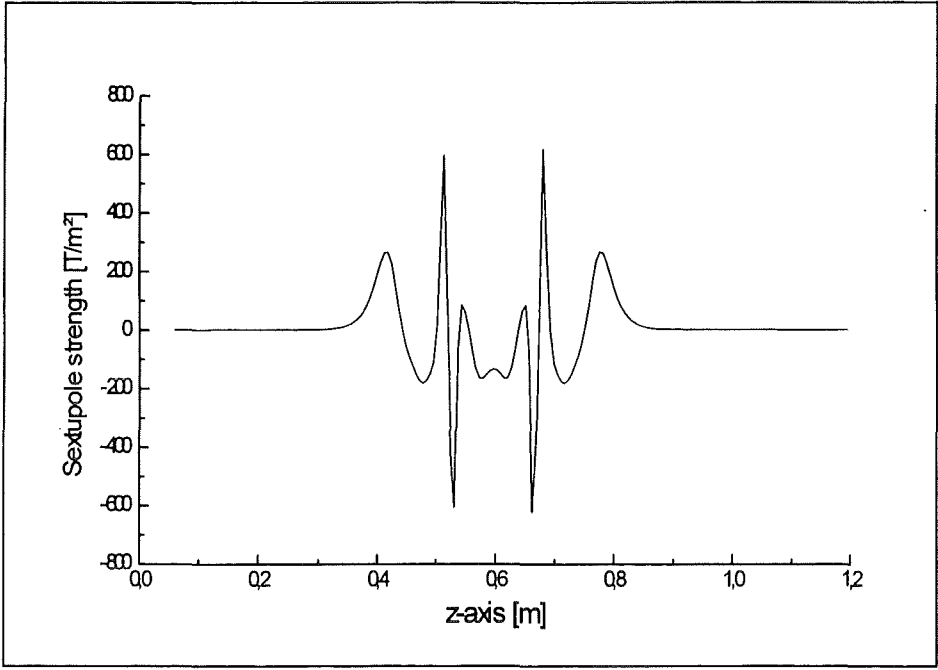Fig. 6: Quadrupole coefficient a_2 as defined in (22).

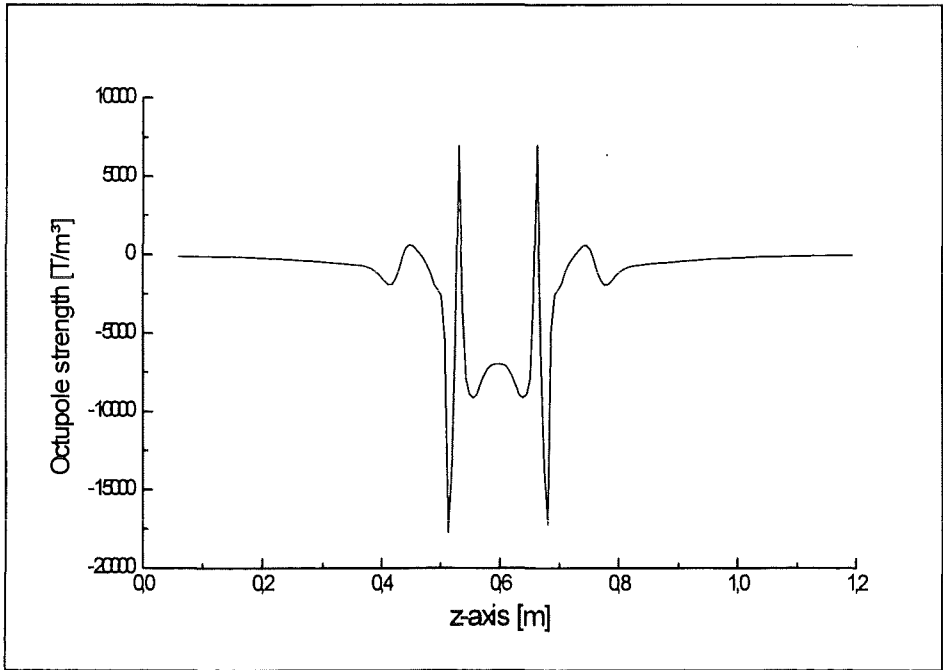Fig. 7: Sextupole coefficient a_3 as defined in (22).

Fig. 8: Octupole coefficient a_4 as defined in (22).

13

TOSCA and a routine using the output files of TOSCA calculates these so-called "Fourier coefficients". The coefficients along the z-axis are shown in figs. 5 to 8 (zero has been shifted compared to figs. 3 and 4 to 0,6 m, the center of the solenoid).

A comparison of figs. 4 and 5 shows that the dipole coefficient a_1 is dominating: the split pair magnet mainly behaves like a dipole. The quadrupole coefficient a_2 has a minimum at the center of the field. The superposition of the fields from the individual coils produces a strong variation of the quadrupole coefficient near the field dip (fig. 6). Figs. 7 and 8 (sextupole and octupole term) show the same strong variation in the vicinity of the field dip as the quadrupole term does. For a net action on the trajectory the integral of the field and the betatron phase advance has to be considered.

It has to be kept in mind that the field components shown in figs. 5 to 8 are not the field components along a particle trajectory but along the z-axis. As a next step the particle trajectory has to be found. This is done with the program ORBIT.

V. The program ORBIT

In the beginning of the calculations the real trajectory, the so-called design orbit is not known. In a first step a trajectory, the so-called reference orbit, which is close to the final design orbit has to be chosen. As a first approximation the beam enters the field via a leading drift space, describes an arc, and leaves it via a trailing drift space. The center of the magnetic field element is positioned at a certain point in the x, z plane (fig. 9).

Input parameters of the program are the strength of the magnetic field, the length over which the field acts and the energy of the electrons (in the following the energy is assumed to be 2.5 GeV). The program calculates the bending radius in the arc section.

$$R = 3.34 \frac{E}{B_{max}} \tag{23}$$

R is the radius in m, E the electron energy in GeV and B_{max} the maximum magnetic field in Tesla. All calculations are performed in double precision.
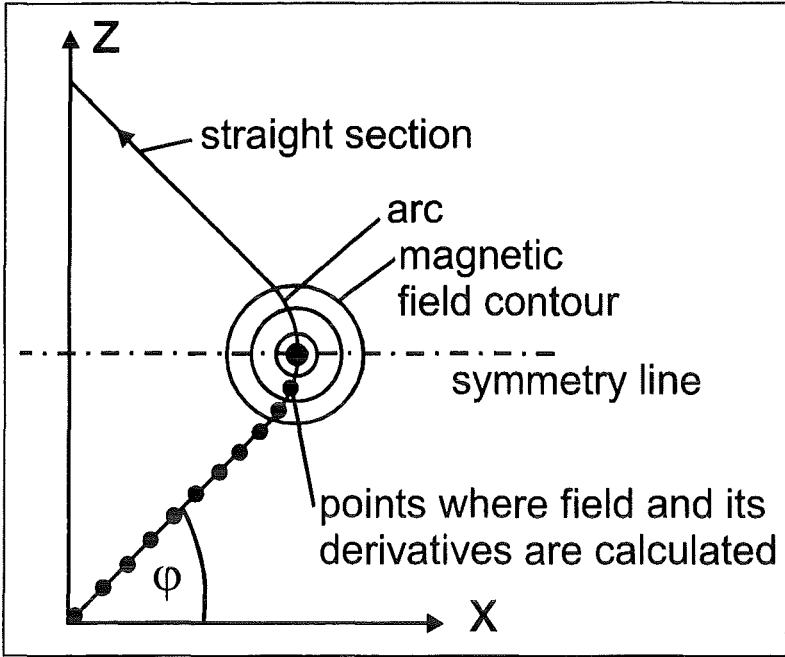
Fig. 9: The reference orbit. The magnetic element is positioned in the positive x, z plane. There are leading and trailing drift spaces. In the reference orbit the beamline element is considered isomagnetic. The trajectory is approximated by an arc with a constant curvature.

The total deflection angle is given by

$$\alpha = 0.3 \frac{180}{\pi} \frac{\int B \cdot dl}{E} \tag{24}$$

α is the total deflection angle in degrees and $\int B \cdot dl$ is the integrated field in Tm along the design orbit. The arc length is

$$arcl = \alpha \frac{\pi}{180} R \tag{25}$$

The field is calculated with TOSCA and an additional program according to equation (22) in the following way. Along the reference orbit equidistant points are selected and the field along

15

a line perpendicular to the design orbit is developed according to equation (22). These values are stored. In order to allow interpolations between the points for each field coefficient a_i a third order spline fit is performed and the spline coefficients are stored.

The spline function algorithm is described in more detail in [10]. Through the given field values a function

$$S = a_i + b_i(x - x_i) + c_i(x - x_i)^2 + d_i(x - x_i)^3 \qquad (26)$$

is fitted where i describes the interval. The coefficients can be evaluated by recursion formulas as shown in appendix III where the w_i are defined as weight functions which have to be chosen between 0 and ∞ (the higher w the lower the deviation from the actual values).

As will be shown in the next chapter, the element under investigation has to be integrated in the program MARYLIE.

In the example given here the total deflection angle is ca. 15 degrees, the angle φ defined in fig. 9 is therefore ca. 82.5 degrees.

The symmetric solution (incoming angle φ, outgoing angle π-φ) is a special case and the use of the program ORBIT is not limited to a symmetric solution.

In order to find a symmetric solution, the program offers an optimization routine. The use of this routine is demonstrated for the split pair solenoid. In order to obtain a symmetric solution, the value of Δp_x can be varied. However other possibilities exist, too. For instance, it is possible to choose a certain start angle and vary the strength of the field until a symmetric solution is found. This procedure is described in the following.

The concept can be described by using the results from fig. 10. One condition for obtaining a symmetric solution is that p_x is zero at the maximum of the field (figs. 9 and 10). In addition, a second condition has to be fulfilled: x has to be identical at the beginning and the end of the trajectory (fig. 11). In principle the two goals have to be reached by iterations since both are connected in a complicated way. First of all, p_x in the center of the trajectory is iterated until it is very small. Afterwards the center of the field is slightly shifted along the x-axis until x is almost zero.

$p_{x,center}$ is the momentum in the x-direction at the center of the field. In order to minimize $p_{x,center}$ the program runs through the following iteration loop

$$B_{new} = B_{old} (1+3.165 \; p_{x,center}) \tag{27}$$

where B_{old} is the magnetic field before iteration, B_{new} is the iterated field and $p_{x,center}$ is the momentum in the x -direction in the center of the field. The logic behind the use of formula (27) is obvious: a negative $p_{x,center}$ requires a smaller field and vice-versa. The value of 3.165 is chosen in a semi-empirical way: with this value the optimization converges fairly rapidly. When $p_{x,center}$ is smaller than a pre-chosen value the program stops.

The result of such an optimization run is shown in fig. 10.
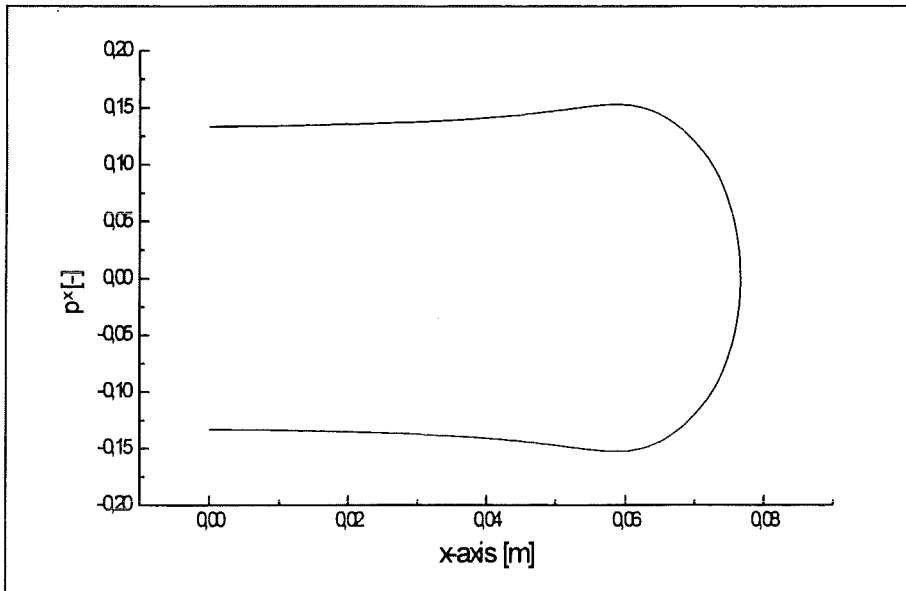
Fig.10: Momentum in the x-direction along the trajectory after an optimization run. $p_{x,center}$ is zero in the center of the trajectory. The particle starts in a drift space at x = 0 (upper part of the curve) with a constant p_x. p_x is bent to the left by the negative field and afterwards towards the right by the main field.

The optimized trajectory shown in fig. 11 is discussed in more detail in the following. A comparison between fig. 4, fig. 10 and fig. 11 shows, as one would expect, that the trajectory is first slightly bent away from the z-axis by the negative field and afterwards bent by the

central field towards the z-axis. The starting angle is chosen so that input and output angle are almost identical.

The influence of the field dip in fig. 4 is hardly visible. In order to calculate the influence of the dip on the trajectory, the field derivatives along the trajectory have to be evaluated. The field derivatives of the field along the trajectory show the influence of the nonlinear field components.

The choice of a different starting angle changes the trajectory and the strength of the nonlinear fields along this new trajectory.

Figs. 12 to 15 show the influence of the nonlinear field along the trajectory.
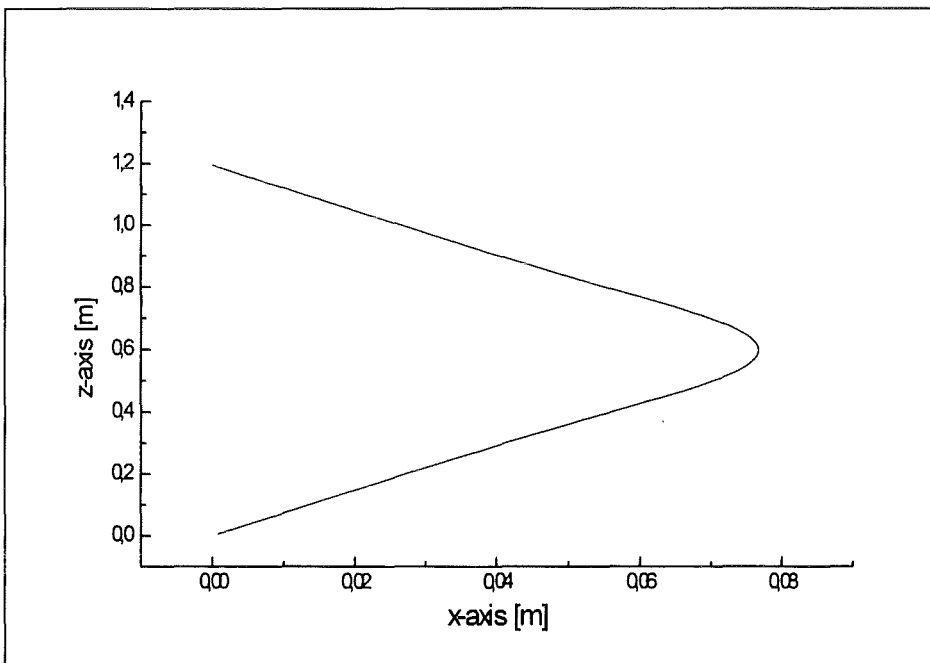
Fig. 11: Optimized trajectory of an electron through the magnetic field of a superconducting split pair solenoid magnet. The incoming and the outcoming angles are almost identical, start point is zero and end point of the trajectory is very close to x = 0 $(8*10^{-7}$ m).

The complete field along the trajectory (fig. 12) is very similar to the field shown in fig. 4. This is not surprising since the start trajectory (fig. 9) is not very far away from the real trajectory. The integrated field strength is 2,23 Tm and depends on the actual trajectory. The

figure is somewhat higher than the figure obtained by integrating the field along a straight line through the center of the field: 2,18 Tm.

Fig. 13 shows the first derivative of the field along the trajectory in x and z direction. At the position of the dip the curves have peaks. The first derivatives $\partial B/\partial z$ and $\partial B/\partial x$ are a measure of the quadrupole content of the field. Integrating along the trajectory, $\partial B/\partial z$ is zero. This is understandable since the trajectory is symmetric. $\partial B/\partial x$ integrated over the trajectory yields a finite value (also understandable as the trajectory is symmetric) and gives rise to a focusing term. Again, the focal strength depends on the trajectory and especially on the symmetry of the trajectory. Similar statements are true for the higher derivatives. When the integral is zero the effects almost cancel. Only when the integral deviates from zero a measurable optical effect is expected.

From this statement it becomes clear that the symmetry in the trajectory greatly reduces the nonlinear effects. As mentioned before, the program also allows to calculate the full influence of the nonlinear effects in the vicinity of the symmetric orbit. This has to be done in order to investigate the full influence of the nonlinearities on the trajectory caused by magnet misalignments.

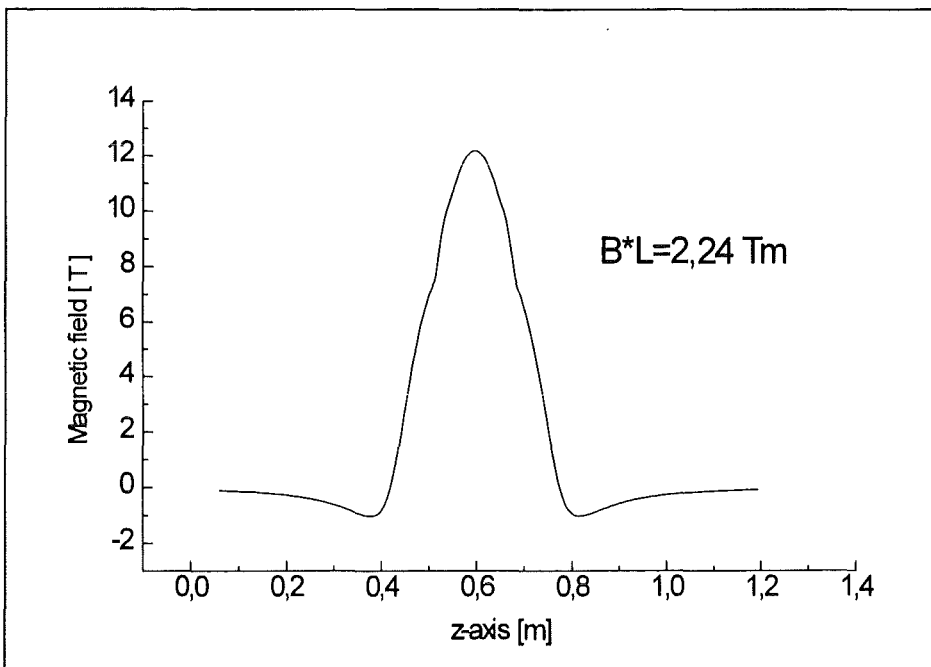

Fig. 13: Transverse magnetic field along the trajectory.

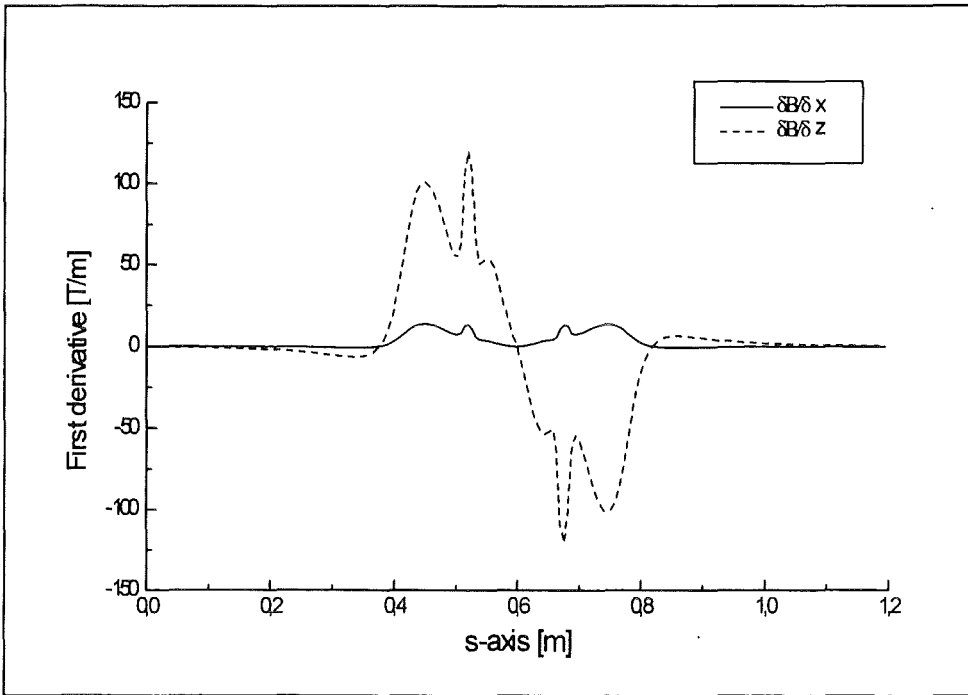Fig. 13: First derivative $\partial B/\partial z$ and $\partial B/\partial x$ along the trajectory s. The integral value of $\partial B/\partial z$ is zero, the integral value of $\partial B/\partial x$ is finite and focuses the beam.
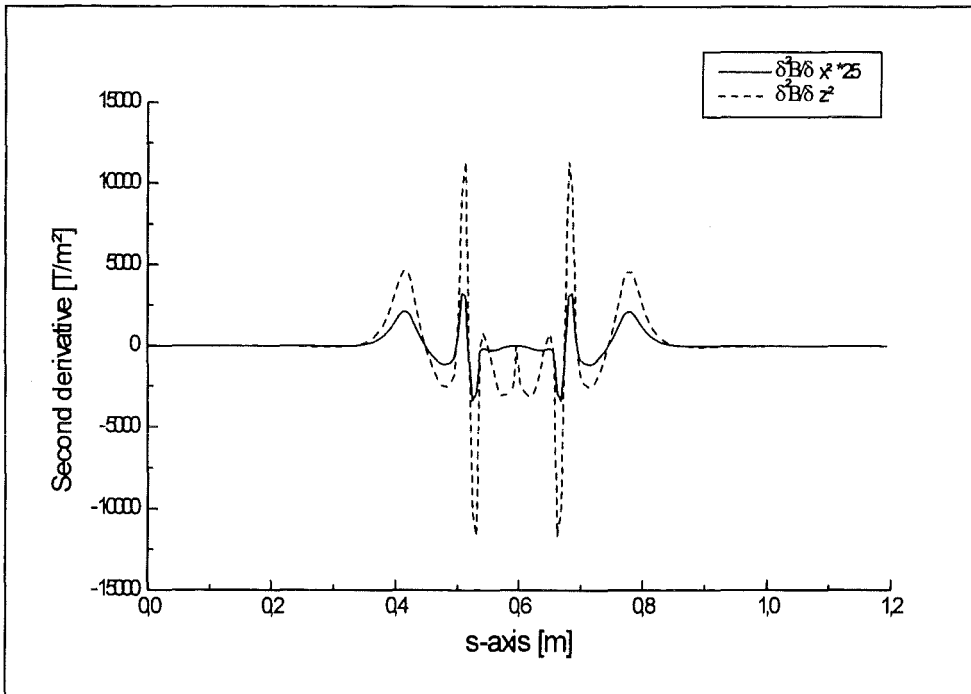
Fig.14: Second derivatives $\partial^2 B/\partial z^2$ and $\partial^2 B/\partial x^2$ along s.

20
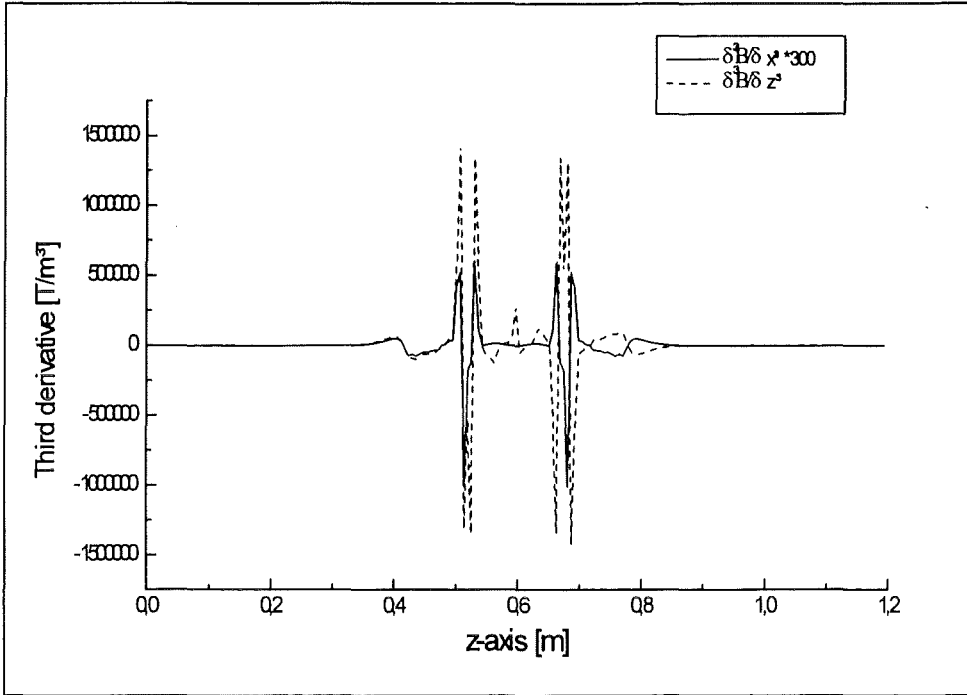
Fig. 15: Third derivatives $\partial^3 B/\partial z^3$ and $\partial^3 B/\partial x^3$ along the trajectory.

VI. The program LIEMAP

After optimization of the trajectory in ORBIT, the program LIEMAP calculates the symplectic transfer map as explained in chapter II. The basic steps are:

a.) Evaluation of the field values and their derivatives along the trajectory.

b.) Generation of the polynomials according to [11].

The output consists of 209 nonlinear coefficients including the linear 6x6-matrix.

In the given example the matrix is

$$
\begin{pmatrix} x \\ p_x \\ y \\ p_y \\ \tau \\ p_\tau \end{pmatrix} =
\begin{pmatrix}
9.385.10^{-1} & 1.168 & 0.000 & 0.000 & 0.000 & -1.614.10^{-1} \\
-1.021.10^{-1} & 9.385.10^{-1} & 0.000 & 0.000 & 0.000 & -2.679.10^{-1} \\
0.000 & 0.000 & 1.004 & 1.207 & 0.000 & 0.000 \\
0.000 & 0.000 & 7.024.10^{-3} & 1.004 & 0.000 & 0.000 \\
2.679.10^{-1} & 1.614.10^{-1} & 0.000 & 0.000 & 1.000 & -6.052.10^{-4} \\
0.000 & 0.000 & 0.000 & 0.000 & 0.000 & 1.000
\end{pmatrix}
\begin{pmatrix} x_0 \\ p_{x0} \\ y_0 \\ p_{y0} \\ \tau_0 \\ p_{\tau0} \end{pmatrix}
$$

21

The focusing strength in both directions is small due to the symmetry of the strong field. For comparison, the focussing strength of a normal ANKA quadrupole is 7 to 8 times bigger. The coefficients in the map are all related to polynomials. The meaning of the coefficients of a polynomial is explained by way of an example in equations (16) and (17). In the following step, the coefficients with the highest values together with the parameters building the polynomial are printed. Polynomials consisting of three elements refer to sextupoles and polynomials consisting of four elements to octupoles.

$F(43) = -0.164$ x, p_y, p_y

$F(53) = -0.546$ p_x, p_y, p_τ

$F(58) = 0.105$ p_x, p_y, p_y

$F(63) = -0.149$ p_x, p_τ, p_τ

$F(76) = -0.621$ p_y, p_y, p_τ

$F(96) = 0.108$ x, x, x, p_x

$F(109) = -0.116$ x, p_x, p_x, p_τ

$F(110) = 0.108$ x, p_x, y, y

$F(111) = 0.124$ x, p_x, y, p_y

$F(132) = -0.136$ x, p_y, p_y, p_τ

$F(140) = -0.133$ p_x, p_x, p_x, p_x

$F(149) = -0.309$ p_x, p_x, p_y, p_y

$F(154) = -0.586$ p, p_x, p_τ, p_τ

$F(161) = 0.138$ p_x, y, p_y, p_τ

$F(174) = -0.154$ $p_x, p_\tau, p_\tau, p_\tau$

$F(175) = -0.415$ y, y, y, y

$F(176) = -10.00$ y, y, y, p_y

$F(179) = -9.057$ y, y, p_y, p_y

$F(185) = -3.657$ y, p_y, p_y, p_y

$F(195) = -0.706$ p_y, p_y, p_y, p_y

$F(200) = -0.637$ p_y, p_y, p_τ, p_τ

LIEMAP is using the cartesian coordinate system x-z defined in fig. 9. MARYLIE uses the standard Frenet-Serret system of coordinates moving with the particle. A coordinate transformation provided by the MARYLIE code has to be applied. When the trajectory is fully symmetric the coordinate transformation is shown in fig. 16.
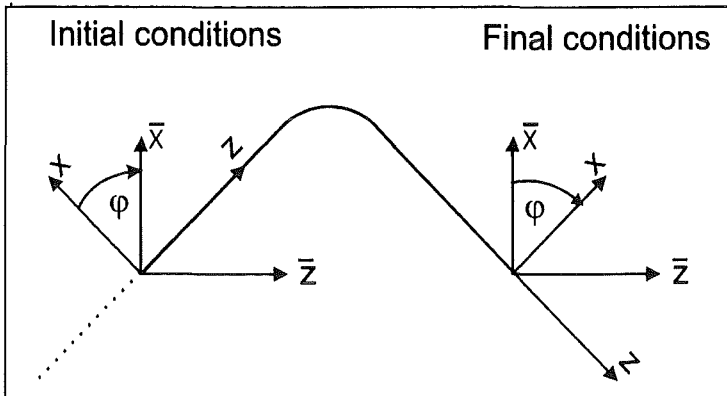
Fig. 16: Transformation from the cartesian system of coordinates $\bar{x}$-$\bar{y}$ used in LIEMAP to the moving coordinate system used in MARYLIE.

VII. The integration of the split pair solenoid magnet into the ANKA lattice

The split pair solenoid magnet is integrated into the standard ANKA insertion section (fig. 17). The normal 22.5 degree bends are followed and preceeded by a triplet (fig. 18). The low horizontal beta is required to avoid an emittance blow-up. The split pair magnet deflecting the beam by 15.3 degrees is surrounded by two 7.65 degree normal conducting isomagnetic bending magnets with a field of 1.5 T each.
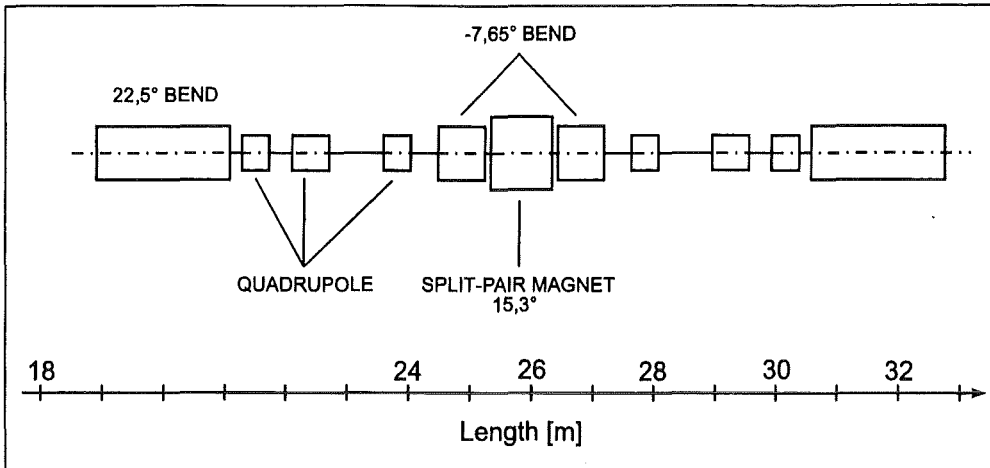
Fig. 17: The insertion section in ANKA for the split-pair solenoid magnet.

In order to keep the emittance low the three bending magnets have to be very close to each other in order to minimize the dispersion in the split pair solenoid magnet. In principle, the two 7.65 degree bending magnets can also be superconducting magnets. This could help to compensate part of the nonlinear effects of the split-pair magnet [12]. Such arrangements are under consideration.
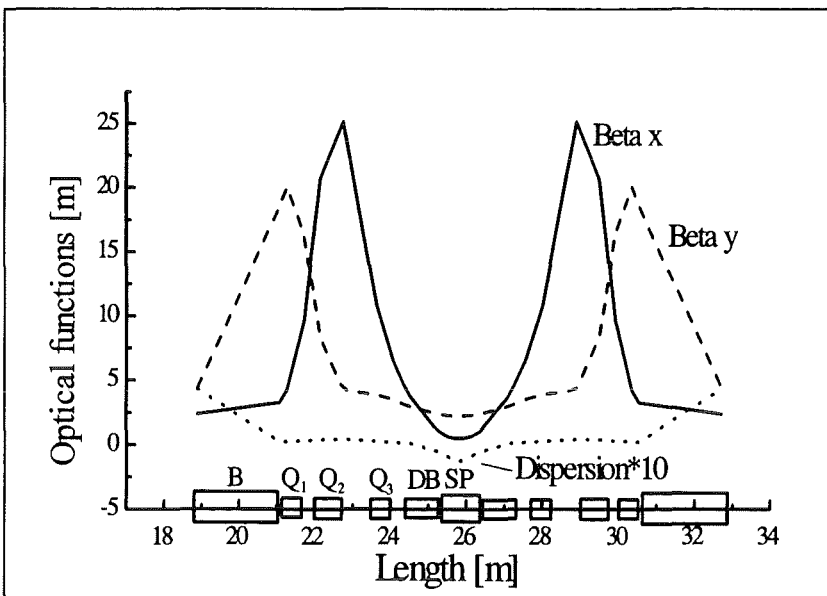
Fig. 18: The optical functions in the insertion device with the split pair solenoid magnet. Solid line: horizontal beta function. Dashed line: vertical beta function. Dotted line: horizontal dispersion.

VIII. The evaluation of the dynamic aperture

The program MARYLIE is used in order to calculate the dynamic aperture of the whole machine including the insertion device as shown in figs. 17 and 18. The map of the split pair solenoid is read by MARYLIE from the LIEMAP output file and integrated into the program.

As already mentioned LIEMAP and MARYLIE are using a different coordinate system a coordinate transformation provided by the MARYLIE code has to be applied.

With MARYLIE the dynamic aperture both with and without the split pair solenoid as an insertion device was calculated. The results of the calculations are shown in figs. 19 and 20. A comparison of both figures shows that the dynamic aperture is mainly limited by the sextupoles of the whole machine. The influence of the split pair solenoid magnet is rather small: The dynamic apertures in both cases are very similar.
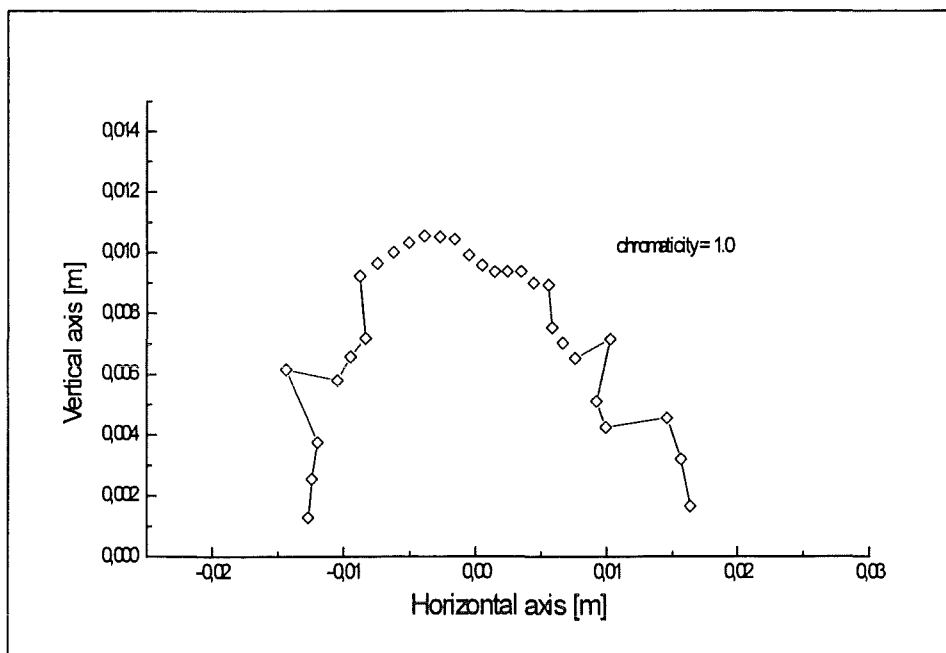
Fig. 19: Dynamic aperture of ANKA without a split-pair magnet.
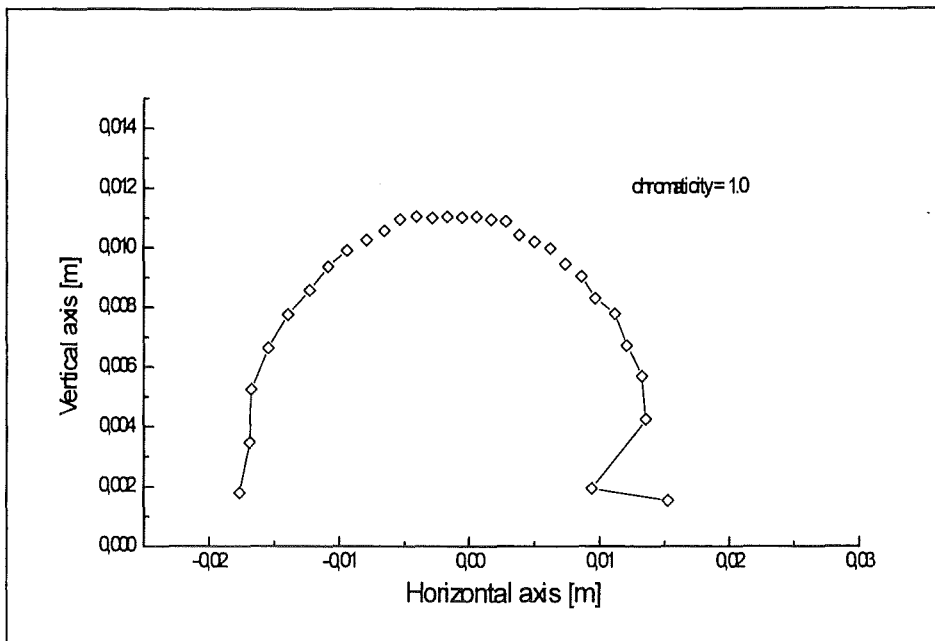
Fig. 20: Dynamic aperture of ANKA with one split-pair magnet.

IX. Brilliance with the split-pair solenoid

In fig. 21 for ANKA the brilliance of a 12 T split pair solenoid and a normal bending magnet as a function of the wavelength is shown. Note that the optical functions are different. The critical wavelength is shifted by a factor of 8 to shorter wavelengths. The extension of the available flux to harder photons will be of interest for application such as fluorescence, absorption spectroscopy and tomography.

26
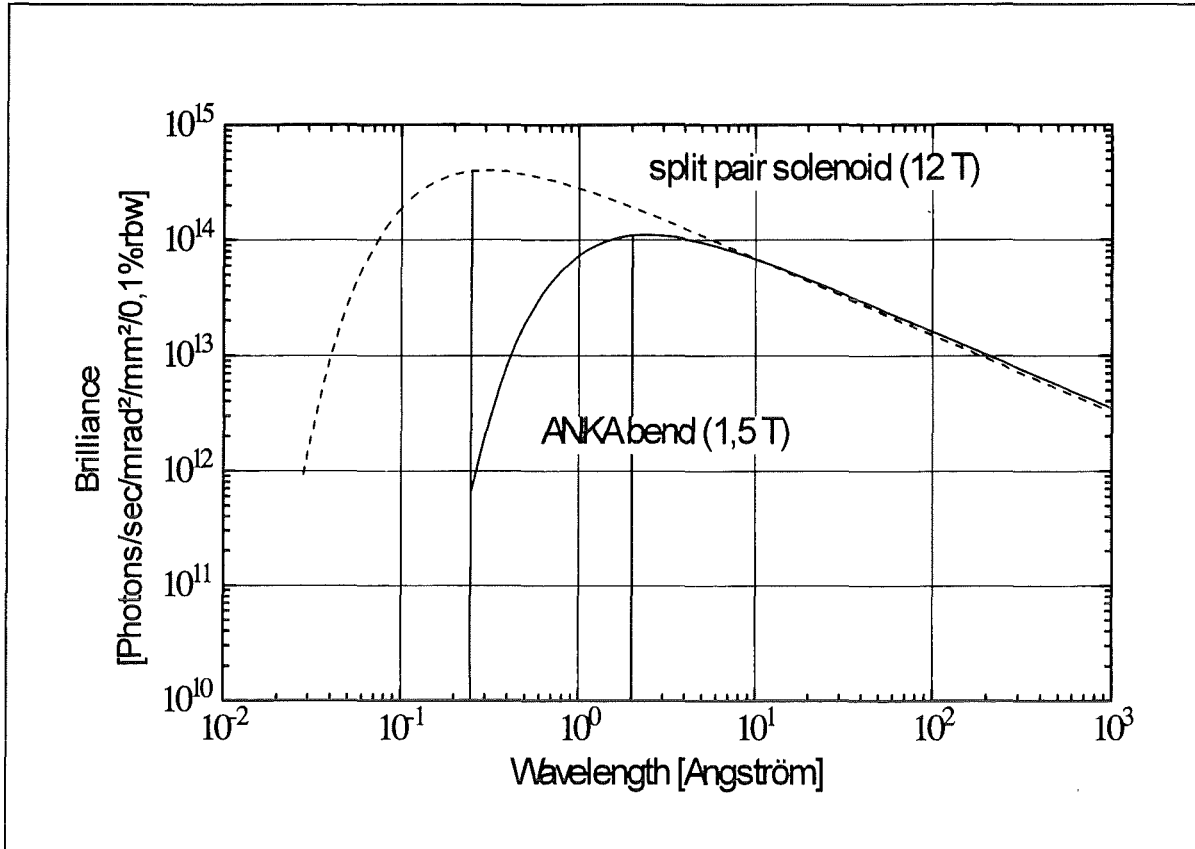
Fig. 21: Brilliance of a 12T split-pair solenoid and a normal bending magnet (1.5 T) as a function of the wavelength. Note that the optical functions are different.

X. Summary

A 12 T split-pair solenoid as an insertion device is investigated using the programs ORBIT, LIEMAP and MARYLIE.

The split pair solenoid can affect the behavior of the storage ring in two ways:

     a.) it can increase the emittance and

     b.) it can decrease the dynamic aperture.

In order to avoid emittance degradation the optical functions in the vicinity of the split pair solenoid have to be chosen very carefully. Both the horizontal beta function and the dispersion have to be small.

27

In order to study the influence of nonlinear effects on the dynamic aperture a method was developed, the use of which is not only limited to a split-pair magnet, but which can also be employed for many other nonlinear insertion device. This technique is based on the Lie-algebra formalism used in various symplectic tracking programs like MARYLIE. The basic idea is to track the particle through this nonlinear field, optimize the trajectory and afterwards find the Lie-map for the nonlinear motion.

The calculations show that it is possible to install a high field superconductive wavelength shifter in a storage ring without unduly disturbing the performance of the ring.

XI. Literature

[1] H. Wiedemann, Design potential of insertion device storage rings, Conf. Stanford. Proceedings, 1985, Insertion devices for synchrotron sources, Proc. of SPIE, 582, p. 110

D. Schirmer, Design study of a superconducting asymmetric multipole wiggler for the 1.5 GeV storage ring DELTA for variably polarized x-ray synchrotron radiation, Hamburg 1992, Proceedings, High energy accelerators, vol. 2, 644-646

H. H. J. ten Kate, D. ter Avest, A. Ravex, M. Lagnier, P. Elleaume, Predesign study of a 4-T to 5-T superconducting wiggler magnet for the ESRF, IEEE Trans. Magn. 30 (1994) 2543-2546

J. P. Jacquemin, J. Perot, Design and test of a 5-T superconducting wiggler, Boston 1987, Proceedings, Magnet technology, 1226-1229

M. W. Poole, J. A. Clarke, P. D. Quinn, S. L. Smith, V. P. Suller, L. A. Welbourne, Commissioning a second superconducting wiggler in the Daresbury SRS, Proceedings of 1993 Particle Accelerator Conference (PAC 93), Washington, DC, 17-20 May 1993, 1638

Y. Fukushima, K. Ohmi, T. Yamakawa, M. Fujiwara, Development of a NB-3SN racetrack magnet for a 10-T superconducting wiggler, KEK-93-5, Jun. 1993, 10pp

A. N. Artemev, A. V. Barkov, A. I. Chechin, A. V. Dudarev, Yu. V. Krylov, N. V. Smolyakov, A 10-T superconducting shifter for the „SIBERIA-2" storage ring, Nucl. Instrum. Methods A308 (1991) 70-72

G. Decker, The superconducting wiggler at the NSLS: systems description and initial experience, Nucl. Instrum. Methods A291 (1990) 357-362)

M. Scheer, Effects of a Superconducting Wavelength Shifter on the Planned Storage Ring BESSY II, Part 1, BESSY TB Nr. 169, November 1992

M. Scheer, G. Wüstefeld, Effects of a Superconducting Wavelength Shifter on the Planned Storage Ring BESSY II, Part 2, BESSY TB Nr. 169, November 1992

P. Gürtler and R. Rossmanith, On the Possibility of Obtaining at PETRA photons with high Brightness at 500 keV and Above, Internal Report, DESY, Hasylab 94-03

[2]   A. J. Dragt, A Method of Transfer Maps for Linear and Nonlinear Beam Elements, IEEE Trans. Nucl. Sc. NS-26, p. 3601

L. M. Healy, A. J. Dragt, I. M. Gjaja, Computation of error effects in nonlinear hamiltonian systems using Lie algebraic methods, J. Math. Phys. 33, p. 1948-1963, 1992

A. J. Dragt, Elementary and advanced Lie algebraic methods with applications to accelerator design, electron microscopes, and light optics, Nucl. Instrum. Methods A258 (1987) p. 339-354

A. J. Dragt, J. M. Finn, Lie series and invariant functions for analytic symplectic maps, J. Mathematical Phys. 17, (1976) p. 2215-2227

[3]   A. J. Dragt, R. D. Ryne, L.M. Healey, F. Neri, D. R. Douglas and E. Forest, MARYLIE program handbook

D. R. Douglas, A. J. Dragt, MARYLIE: The Maryland Lie algebraic transport and tracking code, IEEE Trans. Nucl. Sci. 30 (1983) p. 2442-2444

[4]   H. O. Moser, A. J. Dragt, Influence on Strongly curved large-bore superconducting Bending Magnets on the Optics of Storage Rings, Nucl. Instr. Meth. B24/25 (1987), p. 877

[5]   H. O. Moser, B. Krevet, A.J. Dragt, Nonlinear Beam Optics with real fields in compact storage rings, Nucl. Instr. Meth. B30(1988) p. 105

H. O. Moser, B. Krevet, A.J. Dragt, Nonlinear Beam Optics with real fields in compact storage rings, Proc. IEEE Particle Acc. Conf., Washington D.C., March 1977, p. 458

B. Krevet, H. O. Moser, Performance Study of Superconducting Bending Magnets with Iron in a Compact Synchrotron Light Source, KfK Report 4807, 1990

[6]   The TOSCA reference manual, Vector Fields Limited, Oxford, England

[7]   H. O. Moser, D. Einfeld, R. Steininger, ANKA Proposal, Forschungszentrum Karlsruhe, Sept. 1995, unpublished

[8]   R. L. Burden and J. D. Faires, Numerical Analysis, PWS Publishing Company, Boston, 1993

P. Henrici, Elements of numerical analysis, John Wiley and Sons, New York 1965

E. Fehlberg, Classical Fifth-, sixth-, seventh- and eigth order Runge-Kutta formulas with stepsize control, NASA-TR-R-287, Nov. 1968

E. Fehlberg, Neuere genauere Runge-Kutta-Formeln für Differentialgleichungen zweiter Ordnung, ZAMM 40, 252 (1960)

[9]   Information provided by Oxford Instruments

[10]   G. Engeln-Müllges, F. Reutter, Formelsammlung zur numerischen Mathematik mit Standard FORTRAN Programmen, B.I. Wissenschaftsverlag Mannheim, Wien, Zürich, 1960

[11]   A. J. Dragt and E. Forest, J. Math. PHYs. 24 (1983), 2734

[12]   U. Bandow, D. Einfeld, T. Hezel, B. Krevet, H. O. Moser, R. Rossmanith, J. Schaper, Calculation of the dynamic aperture in the ANKA storage ring with a high-field wavelength shifter, Proceedings EPAC96, Sitges, Spain (in print) and Internal report: ANKA TN BES-01/96

XII. Appendix I

This chapter provides a more detailed information on the use of the programs ORBIT, LIEMAP and MARYLIE.

The programs are all running on a PC in MS-DOS.

General syntax of the Input- and Output-files:
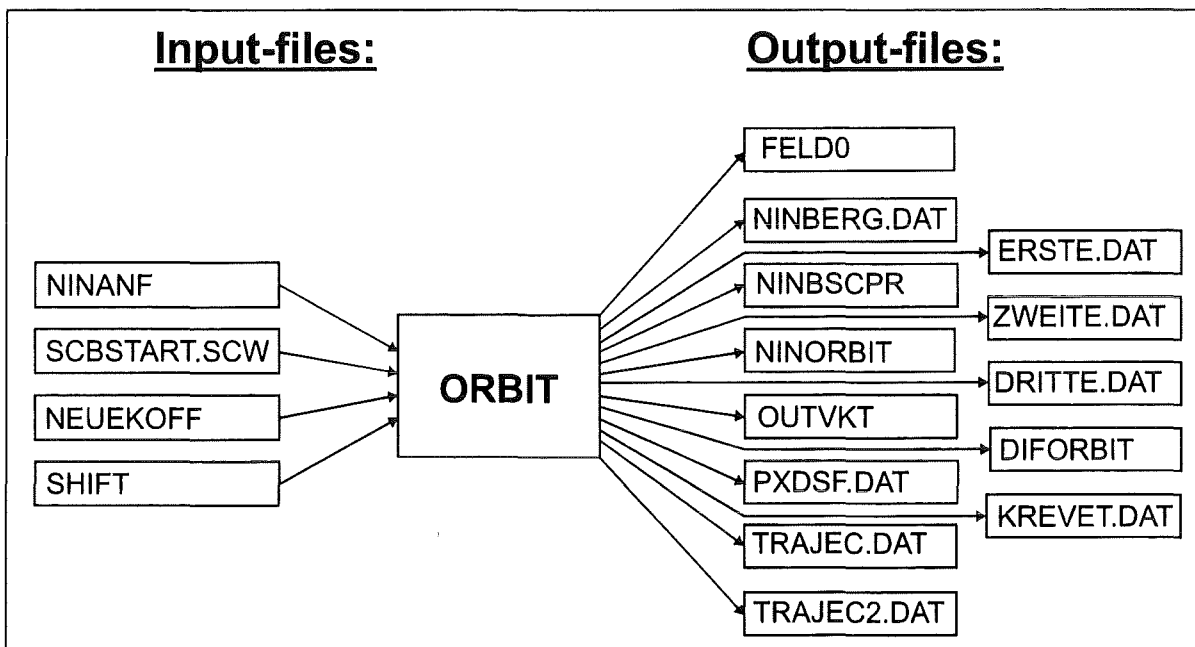
a. ORBIT-files:

Fig. 22: ORBIT input- and output-files.

Input-files:

NEUEKOFF	This file contains the magnetic field, its derivatives and the spline coefficients . The field was numerically calculated by the magnet code TOSCA. In this special case the field is calculated at 151 points starting at the center of the magnetic field. The file consists of two parts: First, the distances between the different points are listed in one column. Secondly, the „Fourier-coefficients" and their spline coefficients are given in four columns and five rows. Both, ORBIT and LIEMAP read this file and reconstruct the field. The first position in this input-file always has to be a zero. This means that the magnetic field is given along a reference orbit which starts in the origin.
NINANF	In this file the user has to provide some basic starting conditions for the program ORBIT. In case of the SPS one should keep the following values: 20 9 5 1.E-9 0 0 0 0 0 0 0 0 20 and 9 are the starting parameters for the Runge-Kutta start up procedure and should not be changed. 5 is the number of steps (NS) and describes the accuracy. EPS was set to 1.E-9. ORBIT compares the momentum in x-direction in the center of the reference orbit and when the momentum is larger than 1.E-9 the maximum magnetic field is changed. The last figure in row one (usually set as zero) enables the user to run ORBIT again with a different starting momentum in x-direction. For every additional ORBIT run one has to add an other row (same syntax as row two). In the second row one can change the starting conditions by varying the initial coordinates and momenta. Syntax: x, p_x, y, p_y, τ, p_τ, z.
SCBSTART.SCW	Syntax: ZINT, DRFT, ARCL, PHI0, SIGN, SL, NS, X0, B0A, DL, FC1, FC2. Units are meter, degrees and Tesla.

	ZINT and X0 define the starting point for the design orbit. DRFT and ARCL represent the length of the driftspace and the arclength. PHI0 is the angle between the driftspace and the x-axis at the starting point. PHI0 should be half of the total deflection angle. SL is a steering parameter and has to be 1. The number of steps (NS) is the same as in NINANF. B0A is the maximum magnetic field DL, FC1 and FC2 are 1.
SHIFT	Syntax: XSHIFT, ZSHIFT. Units are in meter. Steering-file for the programs ORBIT and LIEMAP. By changing the value of XSHIFT and ZSHIFT the center of the reference orbit can be shifted.

Output-files:

DIFORBIT	Syntax: J, DXS, ZDS, SS, B. Units are meter and Tesla. J is a counting variable ranging from 0 to the maximum number of steps (NS). DXS is the difference between the reference and the design orbit in the x-direction. ZDS is the z-component of the design orbit. SS is the length of the trajectory. B is the corresponding magnetic field.
DRITTE.DAT	Syntax: ZDS, D3XB, D3ZB, D3B. Units are meter and Tesla per cubic meter. ZDS describes the z-component of the design orbit. This file shows the third derivatives of the magnetic field in x- and z-direction (D3XB and D3ZB) as well as the sum (D3B). D3XB and D3ZB describe the octupole-strength of the magnetic field.
ERSTE.DAT	Syntax: ZDS, DXB, DZB. Units are meter and Tesla per meter. ZDS describes the z-component of the design orbit. DXB and DZB are the first derivatives of the magnetic field in x- and z-direction. DXB and DZB describe the quadrupole-strength.
FELD0	Syntax: B0A. The unit is Tesla. As already mentioned in the description of NINANF, ORBIT uses B0A

	as the maximum magnetic field.
NINBERG.DAT	Syntax: J, S, S1, B. Unit is Tesla. S and S1 describe the position along the trajectory, B the magnetic field.
NINBSCPR	Syntax: XCNT, ZCNT, RHO, QCS, QSN. Units are meter. This file describes the user chosen reference orbit. XCNT and ZCNT are the cartesian coordinates of the center of the magnetic field. RHO is the radius of the arc in the middle of the reference orbit. QCS and QSN are the cosine and the sine of the starting angle PHI.

NINORBIT	This output-file is divided into two parts:
	
	 1. Syntax: J, XDS, ZDS, DZEQS. Units are meter.
	    XDS and ZDS are the cartesian coordinates of the design orbit.
	    DZEQS is the projection on the z-axis.
	
	 2. Syntax: J, DXB, DZB, D2XB, DXDZB. units are Tesla per meter and
	    Tesla per square meter.
	    These are derivatives of the magnetic field.

OUTVKT	Syntax: I, YR(I), YR(I+1). Output-file of the subroutine OUTVKT. Not used for the present purpose.
PXDSF.DAT	Syntax: XDS, PXDSF. Units are meter. Derivative of the momentum in x-direction of the design orbit.
TRAJEC.DAT	Syntax: XDS, ZDS. Units are meter. The design orbit.
TRAJEC2.DAT	Syntax: ZDS, B. Units are meter and Tesla. The magnetic field along the design orbit.
ZWEITE.DAT	Syntax: ZDS, D2XB, D2ZB, D2B. Units are meter and Tesla per square meter. D2XB and D2ZB are the second derivatives of the magnetic field in x- and z-direction along the design orbit. They represent the sextupole-strength in both directions. D2B is the sum of D2XB and D2ZB.

For practical uses the important output files are TRAJEC.DAT and TRAJEC2.DAT. The rest are expert files to control the program.

b. LIEMAP-files:

Input-files:

FELD0
NEUEKOFF
SCBSTART.SCW
SHIFT

LIEMAP

Output-files:

FELDBERG.DAT
MAP
SPXDSF.DAT
STRAJEC.DAT
STRAJEC2.DAT
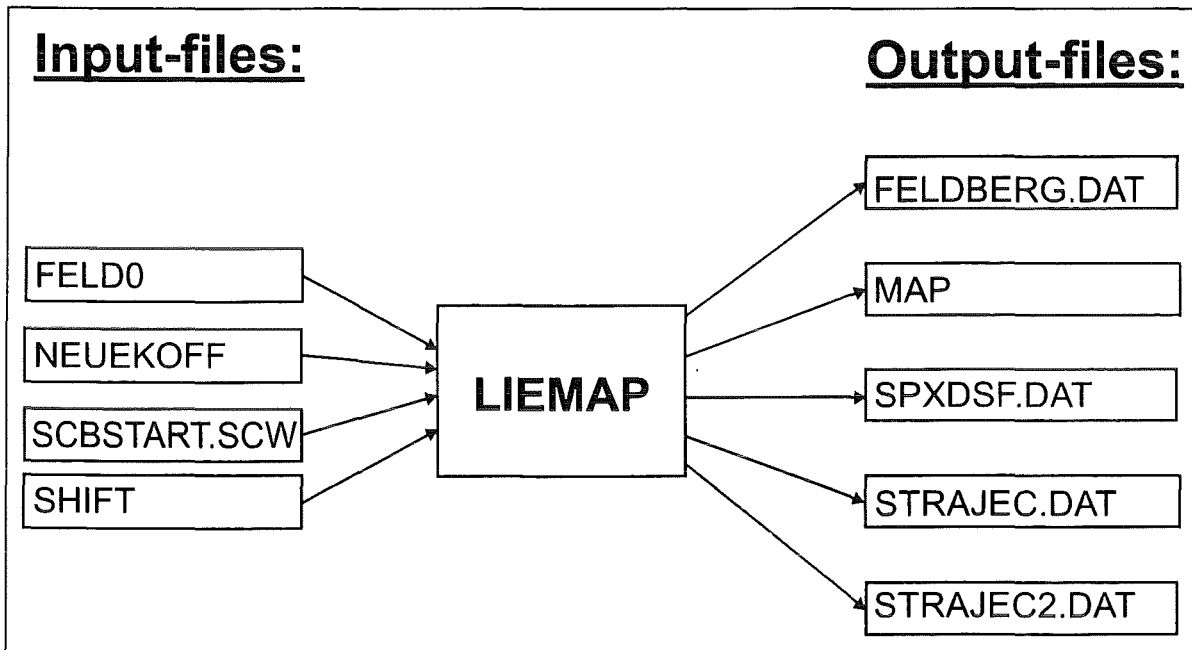
Fig. 23: LIEMAP input- and output-files.

Input-files:

All input-files shown in fig. 23 are identical with the ORBIT input-files.

Output-files:

FELDBERG.DAT	Syntax: J, S, S1, XDS, ZDS, B. Units are meter and Tesla. This file is identical with the ORBIT file NINBERG.DAT. In addition, this file contains the design orbit coordinates XDS and ZDS.
MAP	This output-file is splitted into two parts: 1. Syntax: I, J, M(I,J). Units are dimensionless. 2. Syntax: JK, POL(JK). Units are dimensionless. In M(I,J) the transfer matrix is listed. POL(JK) are the elements of the

37

| | map. This file is used by MARYLIE.

Attention: This transfer map is in the cartesian system of coordinates. It has to be transformed by MARYLIE using the MARYLIE subroutine „plane rotation" (pl). |
|---|---|
| SPXDSF.DAT | Syntax: XDS, PXDSF. Units are meter.

This file is identical to the ORBIT file PXDSF.DAT. |
| STRAJEC.DAT | Syntax: XDS, ZDS. Units are meter.

This file corresponds to the ORBIT file TRAJEC.DAT. |
| STRAJEC2.DAT | Syntax: ZDS, B. Units are meter and Tesla.

This file corresponds to the ORBIT file TRAJEC2.DAT. |

c. MARYLIE-Files:

Input-files: **Output-files:**

Matrix → MARYLIE → DYNAP.DAT

MAP → MARYLIE

MLSTART → MARYLIE → MSG

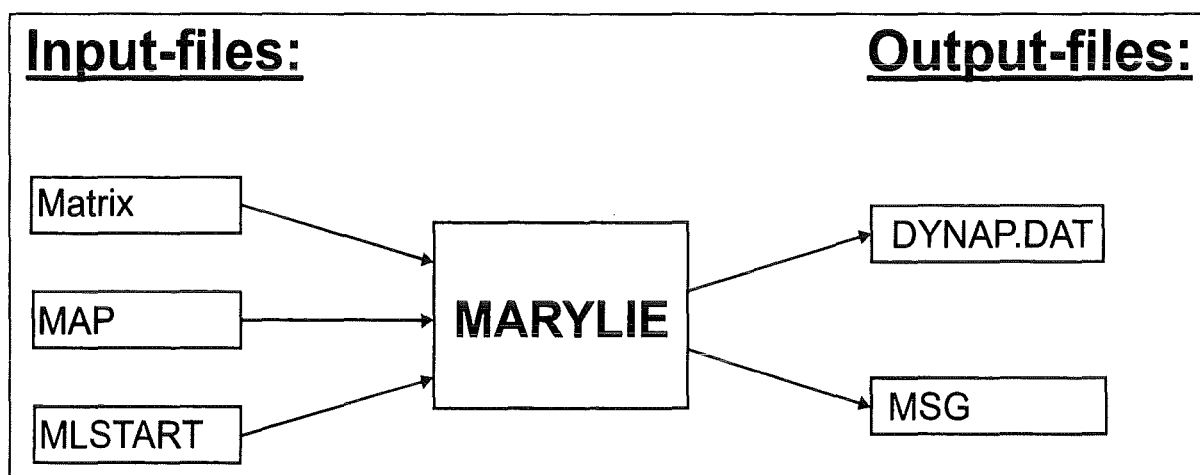Fig. 24: MARYLIE input- and output-files.

Input-files:

MAP	A LIEMAP output-file which has already been described in part b.
MATRIX	MATRIX is used to transform the transfer map saved in the file MAP from the cartesian system of coordinates.
MLSTART	Syntax: 100 0.00001 0. 3.1415927 . Units are radian.

This file is used for the calculation of the dynamic aperture. With this |

	file the user can define some basic side conditions. In this case 100 particles are tracked. The accuracy is 0.00001. The starting angle of the particles varies between 0 and π.

Output-files:

DYNAP.DAT	Syntax: X, Y. Units are meter. This file contains the information about the dynamic aperture where X refers to the horizontal and Y to the vertical axis.
MSG	During a MARYLIE run the complete lattice, the transfer map for the whole machine and optical functions like the chromaticity and the tunes are written into this file. At the beginning of each MARYLIE run the content of this file is deleted and the actual information is written into this file.

d. Example: Simulation of the wavelength shifter

This part of the report shows all input- and important output-files for the simulation of the SPS described in this report.

- NEUEKOFF

```
0.000000
0.155117
..............
..............
64.5679
65.1179
-123751. 215.464 .000000 473.012
-123716. 249.618 220.117 445.390


-0.736047 4.310826E-02 -1.288247E-03 -4.558897E-05
-0.712735 4.164992E-02 -1.363469E-03 8.263518E-04
```

Syntax: First single row: position.

First 4 row line: field and derivatives.

Four lines for spline coefficients, one line for each derivative.

- NINANF   20 9 5 1.e-8 0

                  0.0 0.0 0.0 0.0 0.0 0.0

- SCBSTART.SCW   0.0 0.507 0.186 82.345 1.0 1.0 200 0.0 12.0 0.0 1. 1.
- SHIFT   0.0 0.0
- FELD0   0.118251509054769080E+02
- NINBSCPR   -0.636600 0.597122 0.710468 0.133208 0.991088
- MAP

1	1	0.938491758702784	1	2	1.18857016940871
1	6	-0.459431203271110D-002	2	1	-0.100316497232720
2	2	0.938491784277073	2	6	-0.7491824675483D-02
3	3	1.00423059866773	3	4	1.20715633235319
4	3	0.702395570686947D-002	4	4	1.00423051632730
5	1	0.749189722646328D-002	5	2	0.4592832801898D-02
5	5	1.00000000000000	5	6	0.2168083852443D-01
6	6	1.00000000000000			

28	0.251824746133209D-001	29	0.474967290157914D-001
33	0.300442661531418D-002	34	0.181272645601647D-001
38	0.686344477317820D-001	39	-0.727875581332967D-001
40	-0.913429083037102D-001	43	-0.326738633690888D-001
48	-0.768534281871680D-002	49	-0.936350843317988D-003
53	-0.605623770972478	54	-0.366919706552291D-001
55	0.259754226723167D-001	58	0.264651501003259D-001
63	0.132661691391663D-003	67	-0.527591759741658D-001
70	-0.681339559854452D-001	76	-0.635277823248403
83	-0.113473212798624D-001	84	0.125314118513142D-003
85	-0.492337849709670D-003	89	0.141209510276724D-002
90	0.502461630204337D-002	94	0.598203811694703D-002
95	0.873358921008818D-001	96	0.106126954088461
99	0.331390594251977D-001	104	0.327855882482459D-002
105	0.410554151153510D-001	109	-0.288515984247664D-001
110	0.106149359599646	111	0.109893739809312
114	0.606598300664856D-001	119	0.723520642029755D-001
123	0.154465227817154D-001	126	0.117988978752840D-001
132	-0.111312337301118D-001	139	-0.770397575511330D-002
140	-0.147422252172941	144	-0.170564129143597D-001
145	-0.683985887140526D-001	146	-0.947577432024140D-001
149	-0.330108467696288	154	-0.635475254028321
158	0.172251655048009D-001	161	0.151786692597523
167	0.798078963275834D-001	174	0.361174192914094D-003
175	-4.15151681216491	176	-10.0009358305087
179	-9.06070000111382	184	-0.520904150370920D-001
185	-3.66100848434593	190	-0.676966203963606D-001
195	-0.710266059773607	200	-0.654133458388240
209	-0.119198300454818D-001		

- MATRIX

#comment

MARYLIE file in order to explain the integration of a map (mb) into the Frenet-Serret system of coordinates by using the function plane rotation (pl1 and pl2). The resulting total map is then written to an output file (mb1).
#beam
  8.339102400000000
  4892.602000000000
  1.000000000000000
  1.000000000000000
#menu
mb   tmi
  1.00   15.00   1.00   0.00
mb1   tmo
  16.00
pl1   prot
  7.655   1
pl2   prot
  7.655   2
iden   iden
fin   end
#lines
bea8
  1*pl1   1*mb   1*pl2
#lumps
#loops
#labor
  1*bea8
  1*mb1
  1*fin

- MLSTART   100   0.00001   0.00   3.1415927

41

XIII. Appendix II

The Runge Kutta coefficients:

$$\vartheta_1 = 0$$
$$\vartheta_2 = 2/27$$
$$\vartheta_3 = 1/9$$
$$\vartheta_4 = 1/6$$
$$\vartheta_5 = 5/12$$
$$\vartheta_6 = 1/2$$
$$\vartheta_7 = 5/6$$
$$\vartheta_8 = 1/6$$
$$\vartheta_9 = 2/3$$
$$\vartheta_{10} = 1/3$$
$$\vartheta_{11} = 1$$
$$\vartheta_{12} = 0$$
$$\vartheta_{13} = 1$$

A_{ij}	j=1	2	3	4	5	6	7	8	9	10	11	12	j=13
i=1	0	-	-	-	-	-	-	-	-	-	-	-	-
2	2/27	-	-	-	-	-	-	-	-	-	-	-	-
3	1/36	1/12	-	-	-	-	-	-	-	-	-	-	-
4	1/24	0	1/8	-	-	-	-	-	-	-	-	-	-
5	5/12	0	-25/16	25/16	-	-	-	-	-	-	-	-	-
6	1/20	0	0	1/4	1/5	-	-	-	-	-	-	-	-
7	-25/108	0	0	125/108	-65/27	125/54	-	-	-	-	-	-	-
8	31/300	0	0	0	61/225	-2/9	13/900	-	-	-	-	-	-
9	2	0	0	-53/6	704/45	-107/9	67/90	3	-	-	-	-	-
10	-91/108	0	0	23/108	-976/135	311/54	-19/60	17/6	-1/12	-	-	-	-
11	2383/4100	0	0	-341/164	4496/1025	-301/82	2133/4100	45/82	45/164	18/41	-	-	-
12	3/205	0	0	0	0	-6/41	-3/205	-3/41	3/41	6/41	0	-	-
13	-1777/4100	0	0	-341/164	4496/1025	-289/82	2193/4100	51/82	33/164	12/41	0	1	-
i=14	41/840	0	0	0	0	34/105	9/35	9/35	9/280	9/280	41/840	41/840	41/840

42

- The spline recursion formulas

Equations for c_1, c_2,...,c_{n-1}:

$$h_i = x_{i+1} - x_i$$

$$W_i = \frac{6}{w_i}$$

$$H_i = \frac{1}{h_i} + \frac{1}{h_{i+1}}$$

with the auxiliary functions

$$F_1 = \frac{h_0 - \frac{W_0}{h_0^2} - \frac{W_1}{h_0} \cdot H_0}{22 \cdot h_0^2 + \frac{1}{h_0} \cdot (W_0 + W_1)},$$

$$F_2 = \frac{\frac{W_1}{h_0} \cdot h_1}{2 \cdot h_0^2 + \frac{1}{h_0} \cdot (W_0 + W_1)},$$

$$F_3 = \frac{\frac{W_{n-1}}{h_{n-2} \cdot h_{n-1}}}{2 \cdot h_{n-1}^2 + \frac{1}{h_{n-1}} \cdot (W_{n-1} + W_n)},$$

$$F_4 = \frac{h_{n-1} - \frac{W_{n-1}}{h_{n-1}} \cdot H_{n-2} - \frac{W_n}{h_{n-1}^2}}{2 \cdot h_{n-1}^2 + \frac{1}{h_{n-1}} \cdot (W_{n-1} + W_n)},$$

$$G_1 = W_1 \cdot H_0 + \frac{W_0}{h_0} - h_0^2, \qquad G_2 = \frac{W_1}{h_1}, \qquad G_3 = 3 \cdot \left((u_1 - u_0) - \alpha \cdot h_0 \right),$$

$$G_4 = \frac{W_{n-1}}{h_{n-2}}, \qquad G_5 = \frac{W_n}{h_{n-1}} + W_{n-1} \cdot H_{n-2} - h_{n-1}^2, \qquad G_6 = 3 \cdot \left(\beta \cdot h_{n-1} - (u_n - u_{n-1}) \right),$$

The following system of linear equations exists:

$$\left(F_1 \cdot G_1 + 2 \cdot (h_0 + h_1) + \frac{W_0}{h_0^2} + W_1 \cdot H_0^2 + \frac{W_2}{h_1^2} \right) \cdot c_1 + \left(h_1 - \frac{W_1}{h_1} \cdot H_0 - \frac{W_2}{h_1} \cdot H_1 - F_1 \cdot G_2 \right) \cdot c_2 +$$

$$+ \left(\frac{W_2}{h_1 \cdot h_2} \right) \cdot c_3 = 3 \cdot \left(\frac{(u_2 - u_1)}{h_1} - \frac{(u_1 - u_0)}{h_0} \right) - F_1 \cdot G_3,$$

$$\left(h_1 - \frac{W_1}{h_1} \cdot H_0 - \frac{W_2}{h_1} \cdot H_1 - F_1 \cdot G_2\right) \cdot c_1 + \left(2 \cdot \left(h_1 + h_2\right) + \frac{W_1}{h_1^2} + W_2 \cdot H_1^2 + \frac{W_3}{h_2^2} - F_2 \cdot G_2\right) \cdot c_2 +$$

$$+ \left(h_2 - \frac{W_2}{h_2} \cdot H_1 - \frac{W_3}{h_2} \cdot H_2\right) \cdot c_3 + \left(\frac{W_3}{h_2 \cdot h_3}\right) \cdot c_4 = 3 \cdot \left(\frac{\left(u_3 - u_2\right)}{h_2} - \frac{\left(u_2 - u_1\right)}{h_1}\right) - F_2 \cdot G_3 ,$$

$$\left(\frac{W_{i-1}}{h_{i-2} \cdot h_{i-1}}\right) \cdot c_{i-2} + \left(h_{i-1} - \frac{W_{i-1}}{h_{i-1}} \cdot H_{i-2} - \frac{W_i}{h_{i-1}} \cdot H_{i-1}\right) \cdot c_{i-1} +$$

$$+ \left(2 \cdot \left(h_{i-1} + h_i\right) + \frac{W_{i-1}}{h_{i-1}^2} + W_i \cdot H_{i-1}^2 + \frac{W_{i+1}}{h_i^2}\right) \cdot c_i + \left(h_i - \frac{W_i}{h_i} \cdot H_{i-1} - \frac{W_{i+1}}{h_i} \cdot H_i\right) \cdot c_{i+1} +$$

$$+ \left(\frac{W_{i+1}}{h_i \cdot h_{i+1}}\right) \cdot c_{i+2} = 3 \cdot \left(\frac{\left(u_{i+1} - u_i\right)}{h_i} - \frac{\left(u_i - u_{i-1}\right)}{h_{i-1}}\right) , \qquad\qquad i = 3(1)n\text{-}3,$$

$$\left(\frac{W_{n-3}}{h_{n-4} \cdot h_{n-3}}\right) \cdot c_{n-4} + \left(h_{n-3} - \frac{W_{n-3}}{h_{n-3}} \cdot H_{n-4} - \frac{W_{n-2}}{h_{n-3}} \cdot H_{n-3}\right) \cdot c_{n-3} +$$

$$+ \left(2 \cdot \left(h_{n-3} + h_{n-2}\right) + \frac{W_{n-3}}{h_{n-3}^2} + W_{n-2} \cdot H_{n-3}^2 + \frac{W_{n-1}}{h_{n-2}^2} - F_3 \cdot G_4\right) \cdot c_{n-2} +$$

$$+ \left(h_{n-2} - \frac{W_{n-2}}{h_{n-2}} \cdot H_{n-3} - \frac{W_{n-1}}{h_{n-2}} \cdot H_{n-2} + F_3 \cdot G_5\right) \cdot c_{n-1} =$$

$$= 3 \cdot \left(\frac{\left(u_{n-1} - u_{n-2}\right)}{h_{n-2}} - \frac{\left(u_{n-2} - u_{n-3}\right)}{h_{n-3}}\right) - F_3 \cdot G_6 ,$$

$$\left(\frac{W_{n-2}}{h_{n-3} \cdot h_{n-2}}\right) \cdot c_{n-3} + \left(h_{n-2} - \frac{W_{n-2}}{h_{n-2}} \cdot H_{n-3} - \frac{W_{n-1}}{h_{n-2}} \cdot H_{n-2} + F_3 \cdot G_5\right) \cdot c_{n-2} +$$

$$+ \left(2 \cdot \left(h_{n-2} \cdot h_{n-1}\right) + \frac{W_{n-2}}{h_{n-2}^2} + W_{n-1} \cdot H_{n-2}^2 + \frac{W_n}{h_{n-1}^2} + F_4 \cdot G_5\right) \cdot c_{n-1} =$$

$$3 \cdot \left(\frac{\left(u_n - U_{n-1}\right)}{h_{n-1}} - \frac{\left(u_{n-1} - u_{n-2}\right)}{h_{n-2}}\right) - F_4 \cdot G_6 .$$

Calculation of c_0 and c_n:

$$c_0 = \frac{3 \cdot \left(\left(u_1 - u_0\right) - \alpha \cdot h_0\right) + \left(W_1 \cdot H_0 + \frac{W_0}{h_0} - h_0^2\right) \cdot c_1 - \frac{W_1}{h_1} \cdot c_2}{2 \cdot h_0^2 + \frac{1}{h_0} \cdot \left(W_0 + W_1\right)},$$

$$c_n = \frac{3 \cdot \left(\beta \cdot h_{n-1} - \left(u_n - u_{n-1}\right)\right) + \left(W_{n-1} \cdot H_{n-2} + \frac{W_n}{h_{n-1}} - h_{n-1}^2\right) \cdot c_{n-1} - \frac{W_{n-1}}{h_{n-2}} \cdot c_{n-2}}{2 \cdot h_{n-1}^2 + \frac{1}{h_{n-1}} \cdot \left(W_{n-1} + W_n\right)}.$$

Calculation of a_i:

$$a_0 = u_0 + \frac{2}{w_0 \cdot h_0} \cdot \left(c_0 - c_1\right)$$

$$a_i = u_i - \frac{2}{w_i} \cdot \left(\frac{1}{h_{i-1}} \cdot c_{i-1} - \left(\frac{1}{h_{i-1}} + \frac{1}{h_i}\right) \cdot c_i + \frac{1}{h_i} \cdot c_{i+1}\right), \qquad i = 1(1)n-1,$$

$$a_n = u_n - \frac{2}{w_n \cdot h_{n-1}} \cdot \left(c_{n-1} - c_n\right).$$

Calculation of b_i:

$$b_i = \frac{1}{h_i} \cdot \left(a_{i+1} - a_i\right) - \frac{h_i}{3} \cdot \left(c_{i+1} + 2 \cdot c_i\right), \qquad i = 0(1)n-1.$$

Calculation of d_i:

$$d_i = \frac{1}{3 \cdot h_i} \cdot \left(c_{i+1} - c_i\right), \qquad i = 0(1)n-1.$$